2-23-2009

Functional Analysis of CCM3: a gene contributing to cerebral cavernous malformations

Ryan Matthew Hebert
Yale University

Functional Analysis of CCM3: a gene contributing to cerebral cavernous malformations

A Thesis Submitted to the
Yale University School of Medicine
in Partial Fulfillment of the Requirements for the
Degree of Doctor of Medicine

by

Ryan Matthew Hebert

2008

Acknowledgements

This paper would not have been possible without the insight and support from my advisors Murat Gunel MD and Angeliki Louvi PhD. It was through their encouragement and guidance that this project was chosen and this study completed. I would also like to thank Wang Min PhD for the development of CCM3 floxed mouse.

I am grateful to Althea Stillman, who has provided me with invaluable assistance ranging from experimental design to thesis structure.

This research was partially funded by the National Institutes of Health through the Yale School of Medicine Office of Student Research.

Abstract

Cerebral cavernous malformations (CCM) are a group of homogenous lesions in the brain, spinal cord and retina that consist of focal sinusoidal dilatations of vasculature which can lead to devastating life-altering and/or life-ending events such as seizure and hemorrhagic stroke. CCM exhibit compromised blood brain barrier due to perturbed endothelial cell to endothelial cell tight junctions, resulting in chronic hemorrhage. Linkage analysis has led to the identification of three loci which segregate to familial CCM (CCM1, CCM2 and CCM3). Previous studies have identified PDCD10 as the gene responsible for CCM3. Recent in vitro data have implicated PDCD10 in apoptosis and cell proliferation.

Preliminary in vitro experiments demonstrate an increase in apoptosis after overexpression of PDCD10. Introduction of mutations found in human CCM into the above expression vector failed to increase apoptosis. Human umbilical vein endothelial cells (HUVECs) exposed to conditions of serum deprivation increased expression of CCM3 which preceded an increase in cleaved caspase-3. Conversely, inhibition of PDCD10 expression through siRNA led to a decrease in cell death. These experiments have been helpful in evaluating CCM3 function in vitro. To assess the role of CCM3 in vivo, we have tissue-specifically knocked-out CCM3 utilizing Cre-recombinase mediated recombination of loxP-flanked CCM3 in mice. Tie2 and GFAP promoters were used to drive Cre expression in endothelial cells and astrocytes respectively. Our results indicate that CCM3 is important in the endothelium for early vascular development. These mutant embryos exhibited morphology similar to that of CCM1 knockout mice. Mice deficient in CCM3 in astrocytes exhibited dysmorphic features, such as an enlarged brain

and smaller body habitus when compared with control mice. Histologically, cortical layering was perturbed in the mutant mice. BrdU assays suggest that there is a decrease in dividing cells present in the superficial layers of the cortex. Analysis of one adult mutant survivor led to the discovery of a CCM present near the cerebellar-pontine angle. Isolation of astrocytes from GFAP mutant mice revealed similar characteristics to our previous siRNA experiments using HUVECs. Mutant astrocytes were resistant to cycloheximide induced apoptosis as measured by flow cytometry. Our results support the current hypothesis that PDCD10 is a promoter of apoptosis. These results also suggest that astrocytes play a critical role in the formation of CCM.

Table of Contents

Introduction *5*
CCM1 ..... **7**
CCM2 ..... **8**
ICAP and Beta 1-Integrins **10**
CCM3 ..... **12**
Statement of Purpose *13*
Preliminary Data *14*
PDCD10 overexpression promotes cell death **14**
HUVEC PDCD10 expression increases under serum-deprivation **17**
PDCD10 siRNA decreases cell death **19**
GFAP-Cre;CCM3$^{lox/lox}$ mice exhibit multiple developmental abnormalities **20**
Deletion of CCM3 effects proliferation and apoptosis in primary astrocyte culture **23**
Deletion of CCM3 effects integrin dependent cell function **25**
Methods *26*
Results *36*
Tie2cre **36**
GFAPcre **38**
GFAP-Cre;CCM3$^{lox/lox}$ Astrocyte Culture **40**
Activation of β-1 integrin increase caspase-3 expression **40**
Discussion *44*
Mice deficient in endothelial cell CCM3 are similar to CCM1 knockouts **45**
CCM3 in Glial affects cortical layering **47**
GFAP-Cre;CCM3$^{lox/lox}$ astrocyte cultures are resistant to apoptosis **48**
β-1 integrin modulation changed expression of a modulator of caspase-3 ..... **50**
Conclusion *51*
References *53*

Introduction

Vascular malformations of the cerebrum can lead to devastating life-altering and/or life-ending events such as seizure and hemorrhagic stroke. These malformations can be categorized into five groups: arteriovenous malformations, arteriovenous fistulas, venous malformations, capillary telangectasias, and cerebral cavernous malformations. Cerebral cavernous malformations (CCM) are a group of homogenous lesions in the brain, spinal cord and retina which consist of focal sinusoidal dilatations of vasculature. CCM are characterized by a single layer of endothelium, lacking surrounding smooth muscle, elastin and central nervous system (CNS) parenchymal components. Cavernous malformations manifest most commonly in the brain and spinal cord, but retinal and skin malformations are known findings [1], [2]. CCM exhibit compromised blood brain barrier due to perturbed endothelial cell to endothelial cell tight junctions, thus enabling

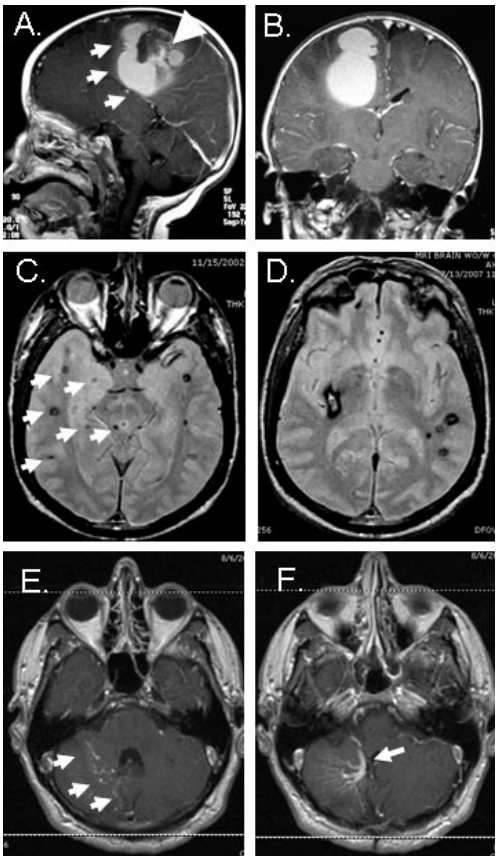

Figure 1 MRI imaging of CCM. *Courtesy of Murat Gunel MD* A. Sagittal & B. Coronal MR images of a large CCM (arrowhead) that caused a gross hemorrhage (white arrows) in a child. C. & D. Axial images of the brain with the genetic form of CCM reveals multiple small hypointense lesions due to hemosiderin (arrows) . E. & F. Axial images show a typical venous malformation with multiple enlarged vessels (arrows) seen after IV administration of contrast material. This patient previously underwent successful surgery for removal of and associated CCM.

red blood cell deposition in adjacent parenchyma. Radiographically, this chronic leakage can be identified by MRI as a hyper-intense ring of hemosiderin deposition surrounding the CCM (Figure 1). Autopsy analyses suggest CCM prevalence to be around 0.5%. CCM make up around 10% of cerebral vascular malformations [3], [4]. Patients presenting with the clinical manifestations of CCM typically present between the third and fifth decades of life with seizure, focal neurological deficit or headache [5]. Seizures represent a common complaint of patients found to have CCM. Studies of patients with CCM reveal seizure as the presenting symptom in fifty to sixty percent of the study groups [5], [6]. Symptomatic hemorrhage rates of CCM seem to be around 3% per patient year with female rates of hemorrhage being higher [7], [6]. CCM are known to occur sporadically, as well as familial. Clinically, these two mechanisms are indistinct, but up to 85 percent of familial cases present with multiple lesions, as opposed to only 25 percent of sporadic cases [8], [6]. CCM location correlates to the proportion of neural tissue through the neuroaxis with approximately eighty percent found supratentorally and roughly twenty percent of lesions found infratentorally [5], [6].

Significant advances have recently been made in understanding the genetic causes of CCM's. Specifically, linkage analysis has led to the identification of three loci which segregate to familial CCM. These loci have been referred to as CCM1, CCM2 and CCM3 [9], [19], [31], [32]. The genes which correspond to these loci have been identified as Krev1/Rap1A Interaction Trapped 1 (KRIT1), MGC4607 (malcavernin) and Programmed Cell Death 10 gene (PDCD10). Although genetic advances have been made, the molecular mechanisms leading to CCM formation, as well as, the temporal and spatial expression pattern and function of KRIT1, MGC4607 and PDCD10 continue to be

unknown. Recent data have implicated these genes in interactions with the extracellular environment and apoptosis.

CCM1

Linkage analysis and mutational screening identified a common mutation in Krev Interaction Trapped 1 (KRIT1) as the genetic source of cavernous malformations in thirty-one of forty-three Hispanic American kindreds originally from northern Mexico [9]. Further analysis of this locus, CCM1, revealed a loss of function mutation of the KRIT1 gene product [10], [9]. Studies using allele specific reverse transcriptase polymerase chain reaction have revealed germ line, as well as, somatic mutations present in malformations, but absent in peripheral blood; suggesting a two-hit hypothesis of CCM formation due to CCM1 [11].

KRIT1 is a small GTP-binding protein originally identified because close homology with the Ras gene and its ability to revert the Ras transformation phenotype [12]. The ability to suppress the Ras oncogene has led to the hypothesis that KRIT1 is a tumor suppressor gene. Analysis of the KRIT1 protein reveals multiple functional domains. Earlier yeast two hybrid screens have identified Krit1 as a Rap1 binding partner [12]. Rap1 regulates integrin activation, formation of cell-cell junctions, cell adhesion [13], [14], [15], [16]. The interaction of Krit1 with Rap1 was confirmed in 2007 by Beraud-Dufour et al. [17]. Using GST pull-down assays, they showed Krit1 preferentially binding GTP-Rap1 through the Krit1 FERM (band four-point-one/ezrin/radixin/moesin) domain. FERM domains are known to allow proteins to interact with plasma membranes by binding plasma proteins and phosphoinositides [18] . In fact, Beraud-Dufour et al reported the ability of Krit1 to bind phosphatidyinositol 4,5-

diphosphate. This study also revealed the interaction of integrin cytoplasmic domain associated protein (ICAP) with Krit1 through an evolutionarily conserved NPxY (phosphor-tyrosine binding domain or PTB) domain present near the N-terminus. Additionally, they provided evidence that the amino and carboxy termini of Krit1 interact in a folded conformation which can be disrupted and straightened by binding to ICAP and that ICAP, Rap1 and Krit1 form a ternary complex in vitro. This leads to the possibility that under certain conditions, Krit1 is transported along microtubules to the plasma membrane where it binds to GTP-bound Rap1, is opened by ICAP and modulates beta-integrin signaling.

CCM2

Although CCM1 accounted for the majority of familial cases of CCM amongst the Hispanic population, familial CCM amongst non-Hispanics was not explained by this locus. In 1998, Craig et al demonstrated linkage of CCM to two new loci in an outbred Caucasian population by genome-wide association studies. These loci were located on the short arm of chromosome 7 (7p15-p13) and the long arm of chromosome 3 (3q25.2-q27) [19]. In 2003 the gene which is responsible for CCM2 was revealed. Liquori et al. [20] sequenced candidate genes found within the boundaries established by Craig et al 1998. This study found eight different mutations in the gene MGC4607 (malcavernin), each mutation, if translated, leading to a truncated gene product and possibly loss of function. Interestingly, like ICAP, malcavernin possesses a phosphor-tyrosine binding domain (PTB) [20].

Concurrent functional studies performed on a newly discovered scaffolding protein revealed an important role in the p38 signalling cascade. It is well established

that the p38 MAP kinase pathway is an important mediator in stress induced cell survival [21], [22]. Uhlik et al (2003) [23] exposed HEK293 cells to a hyperosmotic sorbitol environment in order to activate the p38 MAP kinase pathway. RNAi experiments against MEKK3 inhibited sorbitol induced activation of the p38 MAP kinase pathway. Using MEKK3 as bait in a yeast two-hybrid assay, a small PTB domain containing protein, similar to known adaptor and scaffold proteins, was identified [23]. RNAi knockdown of this gene resulted in near-complete inhibition of sorbitol mediated p38 MAP kinase activation. Immunostaining assays demonstrated the recruitment of this scaffold protein and MEKK3 to dynamic actin under hyperosmotic conditions. The ability of this scaffold protein under hyperosmotic conditions to bind actin, recruit MEKK3 to Rac-GTPase containing sites for modulation of the p38 MAP kinase pathway, led the group to name this protein osmosensing scaffold for MEKK3 (OSM) [23].

Furthermore, CCM2 (OSM) has been directly implicated in CCM1/ICAP/Beta Integrin signaling. CCM2 can be co-immunoprecipitated with endogenous CCM1 in mouse embryonic fibroblast cells [24]. Introduction of a mutation into the CCM2 PTB domain completely prevented co-immunoprecipitation of CCM2 with CCM1. Specifically, the addition of a mutation, known to be present in a CCM kindred (L198R), which lies in the C-terminal area of the PTB domain present in CCM2 abolishes CCM2 co-immunoprecipitation with CCM1. Additionally, mutations introduced into a different NPxY domain on CCM1 known to be important for ICAP binding [25] failed to interfere with CCM1/CCM2 co-immunoprecipitation. This finding leads to the hypothesis that CCM1 binds both ICAP and CCM2 through different NPxY/PTB binding interactions [18] , [24]. The binding of CCM1 partners to different NPxY domains implies that all

three have the potential to form a complex. As predicted, 293T cells transfected with MEKK3, CCM1, CCM2 constructs; immunoprecipitated with CCM2 and then immunoblotted with CCM1 revealed the presence of both CCM1 and MEKK3 [24]. This provides evidence for a protein complex composed of at least CCM1, CCM2 and MEKK3.

mRNA expression and Subcellular localization studies have led to the hypothesis that co-expression of CCM complex constituents can lead to differential sequestration. Overexpression of a CCM1 construct in 293T cells reveals CCM1 existing in both cytoplasmic and nuclear compartments. Overexpression of a CCM2 construct in the same cell line reveals the presence of CCM2 solely in the cytoplasm. Co-expression of both constructs leads to CCM1 exclusion from the nucleus. These findings support the conclusion that CCM2 binds to and sequesters CCM1 in the cytoplasm [24], [26].

ICAP and Beta 1-Integrins

ICAP, like Krit1, contains a nuclear localization sequence. Translocation of ICAP into the nucleus was demonstrated in osteoblasts seeded on beta-integrin substrate (fibronectin) coated plate. ICAP mediated activation of the c-myc promoter and subsequent cell proliferation is dependent on this translocation [27]. Additionally, Overexpression of ICAP causes increased cell motility and adhesion to beta-integrin substrates [28].

Beta-1-integrins are a set of transmembrane receptors which bind the extracellular matrix (ECM) and, on the cytoplasmic side, constituents of the cytoskeleton. Beta-1-integrins are heterodimeric complexes, composed of one beta-1 subunit and one of a number of alpha subunits. Mice lacking expression of the beta-1 subunit in radial glia

exhibit defects in connections of glial foot processes to the basement membrane of the meninges [29]. Studies using a neural progenitor promoter, Nestin, to drive Cre recombinase mediated deletion of beta 1-integrin, Belvindra, et al. [30] provided evidence that neural migration from the ventricular zone to the superficial layers of the cortex was not dependent on beta 1-integrin expression in neurons. Additionally, neuronal projections and pyramidal neuron morphology was not perturbed in the Nestin driven knock-out. In contrast, a mouse completely deficient of beta 1-integrin in the central nervous system exhibits greatly perturbed development of cortical layers and pyramidal neuron morphology; leading to the conclusion that beta integrin expression in radial glia is important for cortical layer and dendritic projection formation and guidance [30].

With this data from CCM1, CCM2, and ICAP studies, one could imagine a mechanism which consists of beta-integrin activation (possibly along with a co-stimulant) leading to CCM1 binding to ICAP and revealing the Talin binding site, allowing Talin to bind and leading to propagation of the beta-integrin signaling cascade modulating cell adhesion and migration. Krit1 binding to ICAP, while also bound to malcavernin, brings malcavernin into close proximity with the plasma membrane where it can bind MEKK3 and modulate the p38 signalling pathway. It would be interesting to know whether (or when) malcavernin dissociates with the Krit1/ICAP complex, allowing Krit1/ICAP to translocate to the nucleus and effect cell proliferation, migration and/or adhesion. Elucidation of this mechanism would fail to address the role of CCM3 in the formation of cerebral cavernous malformations.

CCM3

CCM1 and CCM2 mutations account for around sixty percent of familial forms of the disease [31], [32]. A third locus linked to the familial formation of CCM was discovered in 2005 [31], [32]. This new locus, CCM3, was found to harbor mutations in programmed cell death gene 10 (PDCD10). This gene is member of a family of genes known to be important in regulation of apoptosis. PDCD10 was originally described as being upregulated in a premyeloid cell line after 8 hours of granulocyte-monocyte colony stimulating factor (GM-CSF) deprivation and activation of apoptosis [33]. Subsequent studies have found PDCD10 to be upregulated in skeletal muscle after denervation [34] and in cultured fibroblasts after exposure to cycloheximide [35]. Unfortunately, increased expression of the gene in response to apoptotic stimuli does not explain function as cell survival components could be upregulated, as well as, cell death constituents under apoptotic conditions. siRNA experiments against PDCD10 in human prostate cancer cell line (PC-3) cultures led to decreased proliferation, as measured by a tetrazolium salt assay, over 120 hours. Furthermore, MST4, a Sterile-20 protein kinase, dependent activation of PC-3 proliferation was inhibited by PDCD10 siRNA [36]. MST4 is a known modulator of the extracellular-regulated kinase (ERK) pathway [37]. These results directly implicate PDCD10 in modulation of ERK signaling. It is unclear where PDCD10 lies in the ERK signaling pathway. In the PC-3 cultures experiments, it seems that PDCD10 is downstream of MST4. Another possibility is that PDCD10 is part of a synergistic pathway that, when lost, prohibits the proliferative signals from ERK/MST4 activation. Of interest, integrin signaling has been implicated in the modulation of mitogen activated protein (MAP) kinase/ERK pathway [38]. This data provides insight

into the possible connection between beta integrin activation, PDCD10 and ERK signaling pathway.

CCM3 may bind to CCM2 and its function may be regulated by phosphorylation. Yeast two-hybrid, in vitro co-immunoprecipitation and GST pull downs have identified serine/threonine kinase 25 (STK25) and Fas-associated phosphotase (FAP-1) as binding partners for CCM3. STK25, in vitro, possessed the ability to phosphorylate CCM3. While FAP-1's catalytic domain possessed the ability to de-phosphorylate CCM3 [39]. Overexpression of CCM3 in HEK293 cells along with CCM2 and CCM1 resulted in CCM3 co-immunoprecipitating with CCM2, but not with CCM1 [39]. Additionally, mutations known to be present in familial CCM have been shown to disrupt the ternary CCM complex in vitro [40]. These findings support the hypothesis that CCM3 does not bridge binding of CCM1 to CCM2, but binds directly to CCM2 and not CCM1. The relationship between CCM1 and CCM3 is dependent on CCM2.

Statement of Purpose

The purpose of our experiments is to further elucidate the function of CCM3. We will achieve this by using a conditional mouse knock-out of CCM3. Specifically, we have utilized the bacteriophage derived Cre-recombinase deletion of DNA sequence flanked by sequence specific loxP sites. We have used cell line specific promoters to drive Cre-recombination of CCM3-loxP flanked alleles. A mouse harboring a CCM3floxed allele was generated in the laboratory of Wang Ming PhD (Department of Pathology, Yale School of Medicine). For the endothelial cell knock-out, the Tie2 promoter was used to drive Cre-recombinase. This mouse was developed in the

Yanagisawa lab (UT Southwestern). This promoter is known to drive recombination in endothelial cells present in the embryo, as well as, the yolk sac beginning around e8.5 [41]. Cre-recombination in neural progenitors was driven by the Nestin promoter. This mouse was obtained through Jackson Laboratories and is known to express Cre at embryonic day 11. Astrocytes, oligodendrocytes, ependymal cells and a subset of neurons were targeted for Cre-mediated deletion of CCM3 under the control of the glial fibrillary acidic protein (GFAP promoter). This mouse was obtained from Jackson Laboratories and is known to mediate recombination in the above cell lines by e13.5.

We believe knocking-out CCM3 in cells present in the CNS will lead to CCM formation and possibly an increased number of cells present in the CNS, either by increased proliferation or decreased apoptosis. We have also used human umbilical endothelial cells and primary murine astrocytes exposed pro-apoptotic conditions to study the function of CCM3 in vitro. We believe CCM3 to be important in the apoptotic pathway. Furthermore, we believe the absence of CCM3 will lead to decreased apoptosis.

Preliminary Data (data performed by others in the lab of Murat Gunel MD)

PDCD10 overexpression promotes cell death

Transfection of HELA cells with the construct pEGFP(C3)-hCCM3 led to an increase in terminal deoxynucleotidyl transferase-mediated dUTP nick end-labeling (TUNEL) as compared to HELA cells transfected with an empty GFP construct. HELA cells transfected with a CCM construct displayed morphologic changes consistent with apoptosis, fragmented nuclei, and exhibited increased expression of caspase-3 (Figures 2

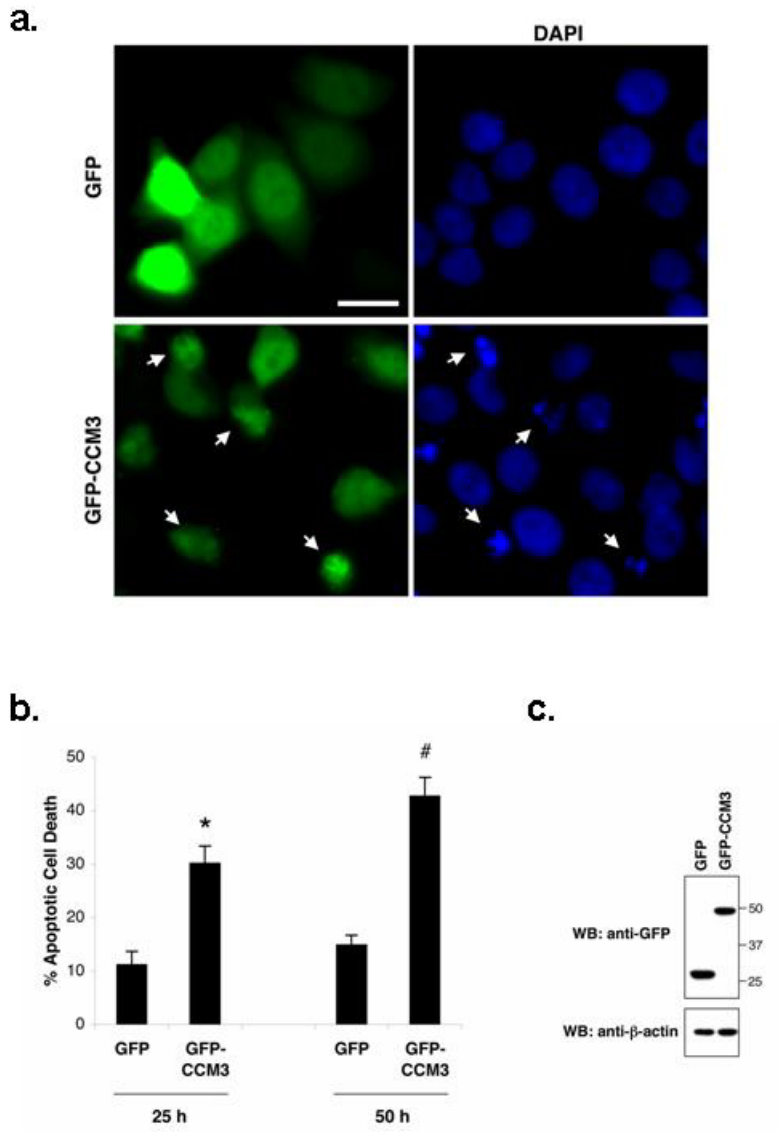

Figure 2 CCM3 induces apoptosis in HeLa cells. *Courtesy of Leiling Chen MD and Murat Gunel MD.* HeLa cells were transfected with GFP-CCM3 or GFP constructs and then serum-starved starting seven hrs after transfection. 50 hrs after transfection, cells were fixed, and nuclei stained with DAPI (blue). Arrows point to the GFP-CCM3-positive cells (green) with condensed or fragmented apoptotic nuclei. Scale bar = 20 μm (a). GFP-positive cells were quantified for apoptosis by scoring apoptotic nuclear morphology as in (a). The percentage of GFP-positive cells with apoptotic nuclei was represented as mean + SEM from three (n = 5) and four (n = 14) independent experiments for the 25 and 50 hr timepoints, respectively (left panel). **P* < 0.002, significant difference from GFP-transfected cells; #*P* < 0.001, significant difference from GFP-transfected cells (by Student's t-test) (b). Protein expression of GFP and GFP-CCM3 25 hrs after transfection was confirmed by immunoblotting with anti-GFP. Anti-actin was used as a control for loading (right panel) (c).

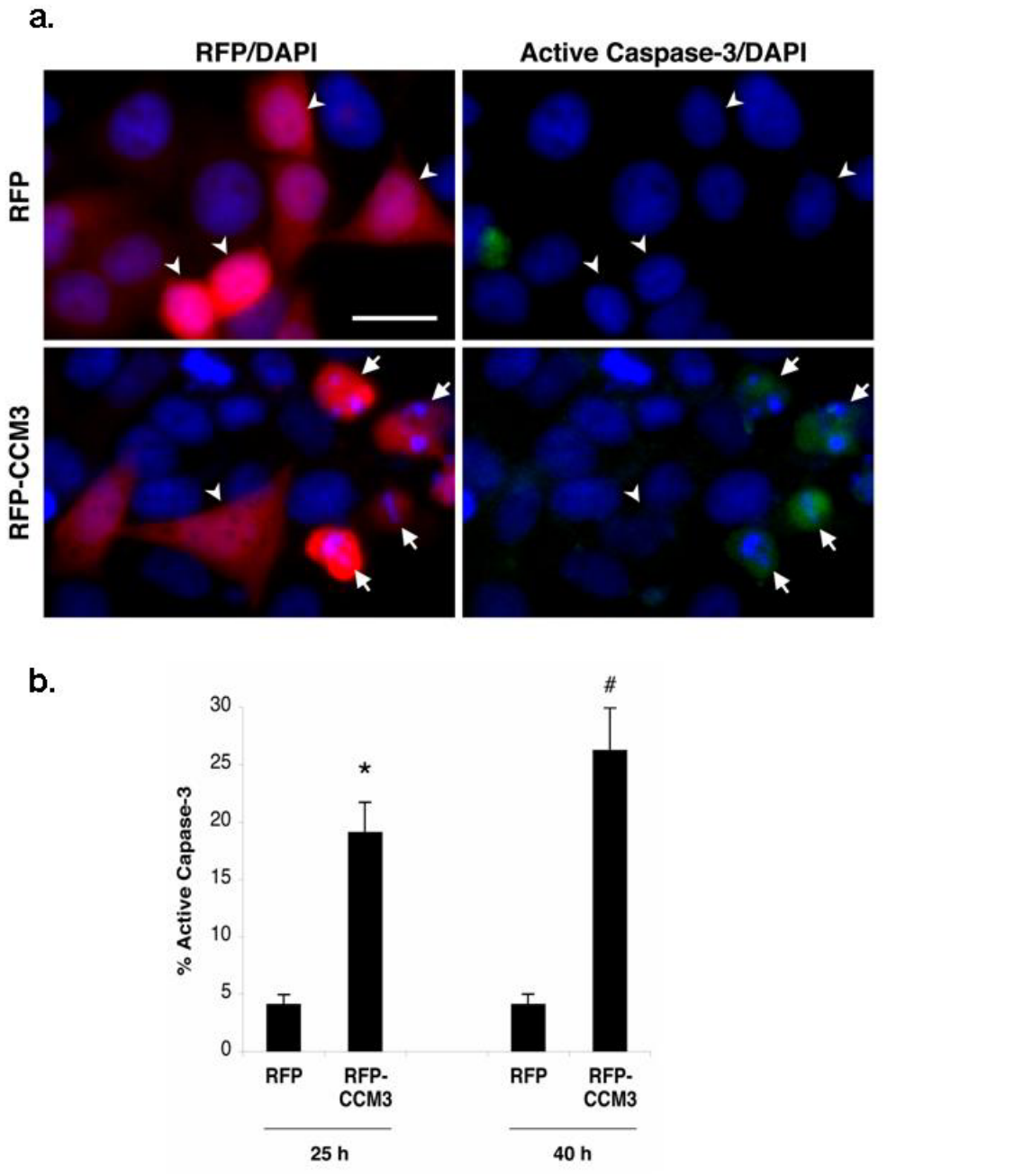

Figure 3 CCM3 activates caspase-3 in HeLa cells. *Courtesy of Leiling Chen MD and Murat Gunel MD.* (a) HeLa cells were transfected with RFP-CCM3 or RFP constructs and then serum-starved starting seven hours after transfection. 40 hrs after transfection, cells were fixed and immunostained with FITC-anti-active Caspase-3 (green), and nuclei were labeled with DAPI (blue). Arrows point to RFP-CCM3-positive cells (red) that are active Caspase-3 immunoreactive. Arrowheads represent transfected cells that are not active Caspase-3 immunoreactive. Scale bar = 20 μm. (b) RFP-positive cells were assessed for Caspase-3 activation by scoring active Caspase-3-immunoreactivity as indicated in (a). Histogram represents mean + SEM from three (n = 7-10) independent experiments for the 25 hr and 40 hr timepoints, respectively. **P* < 0.001, significant difference from RFP-transfected cells; #*P* < 0.001, significant difference from RFP-transfected cells (by Student's t-test).

and 3). This data is consistent with the hypothesis that overexpression of CCM3 leads to apoptosis.

Introduction of mutations reported to be present in kindreds of CCM (c.283C>T and c.194delA), which result in a truncated gene product, into the above expression vector failed to increase the amount of cleaved caspases-3 in HELA overexpression experiments (Figure 4).

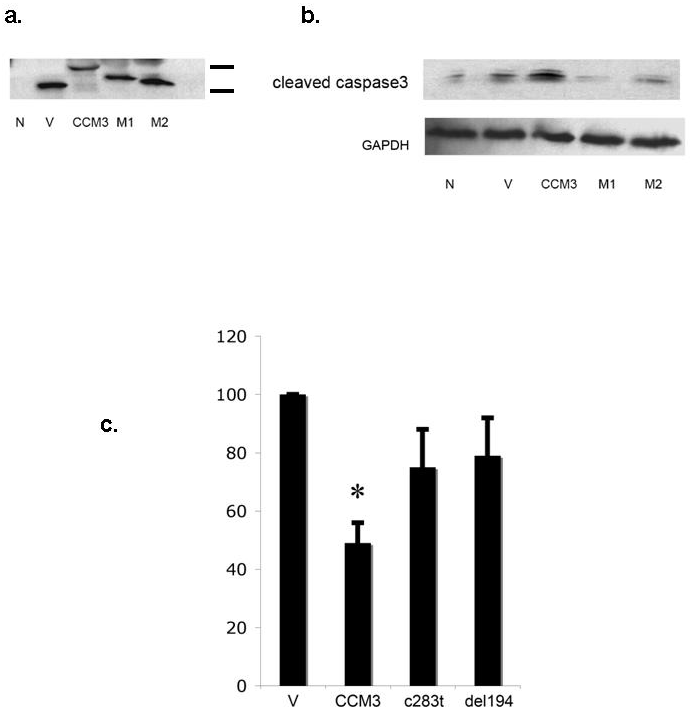

Figure 4 Mutated CCM3 fails to induce apoptosis *Courtesy of Leiling Chen MD and Murat Gunel MD.* (a) Transfection with wildtype CCM3 increases cleaved caspase 3 expression levels, while transfections with either mutated CCM3 construct has no effect on cleaved caspase 3 expression. Legend: N= transfection reagent alone, V= GFP vector alone, CCM3= transfection with wildtype pEGFP-hCCM3 vector, M1 = transfection with pEGFP-hCCM3 vector containing the c.283C>T mutation, M2 = transfection with pEGFP-hCCM3 vector containing the c.194delA mutation. (b) Control western probed for anti-GFP (Sigma Aldrich, MO) demonstrates transfection efficiency. Legend: N= transfection reagent alone, V= GFP vector alone, CCM3= transfection with wildtype pEGFP-hCCM3 vector, M1 = transfection with pEGFP-hCCM3 vector containing the c.283C>T mutation, M2 = transfection with pEGFP-hCCM3 vector containing the c.194delA mutation. (c) Transfections with mutated CCM3 shows reduced cell loss compared to wildtype CCM3. Cell viability was measured using the 3-(4,5-dimethylthiazol-2-yl)-2,5-diphenyl tetrazolium (MTT) assay and is graphed as a percentage of the control culture value (GFP plasmid transfection group) as quantified by determining the absorbance of cell cultures at 550 nm. Asterisk denotes $P < 0.05$ vs. GFP plasmid transfection group.

HUVEC PDCD10 expression increases under serum-deprivation

Human umbilical vein endothelial cells cultured in the absence of fetal bovine serum (FBS) resulted in increased expression of cleaved caspase-3 after three hours (Figure 5a). Interestingly, CCM3 expression preceded the increased expression of cleaved caspases-3.

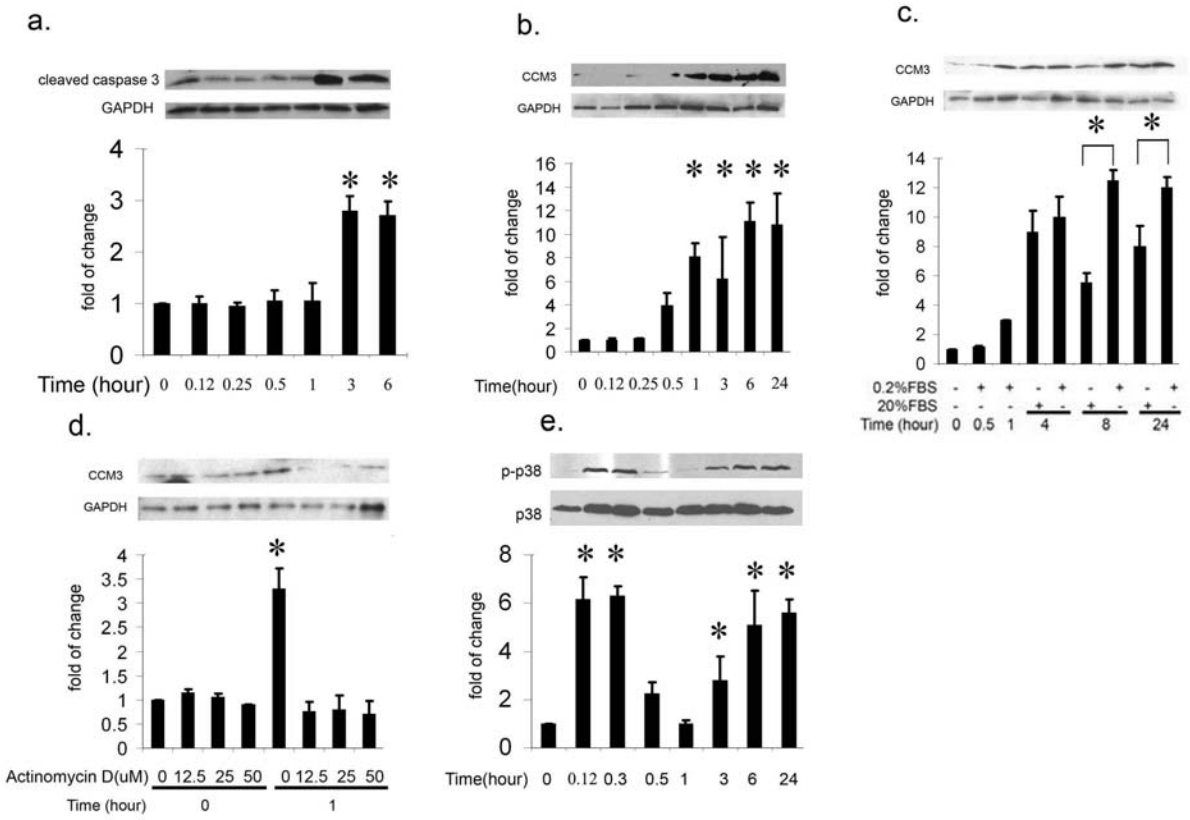

Figure 5 Serum-starved endothelial cells result in apoptosis, increased CCM3, activated Caspase 3, and p38 levels. *Courtesy of Leiling Chen MD and Murat Gunel MD*. (a) Serum-deprived HUVECs demonstrate an increase in cleaved caspase 3 levels by hour 3. Graphed densitometric analysis of cleaved caspase 3 is normalized to GAPDH. (b) CCM3 expression increased upon serum-deprivation starting at approximately 30 minutes, prior to the increase in cleaved caspase-3 levels as demonstrated by (a). (c) Addition of serum to cell culture rescues CCM3 expression. The x-axis denotes the addition (+) or absence (-) of different concentrations of FBS (normal=20%, deprivation=0.2%) over different time points. The graphed densitometric analysis of cleaved caspase 3 is normalized to GAPDH as demonstrated by the western blot above. (d) Cell cultures were incubated with various concentrations of Actinomycin D (x-axis, top), a transcription inhibitor at time=0 and =1 hour (x-axis, bottom). Actinomycin D treatment inhibits CCM3 expression confirming that serum starvation causes an increase in CCM3 transcription. (e) Serum deprivation results in an increase in activated (p-) p38 prior to activated caspase 3 activation as demonstrated by (a). Levels of p-p38 increase dramatically upon serum starvation at 6 minutes, followed by a second peak beginning at 3 hours.

Increased CCM3 expression was noticeable as soon as thirty minutes after withdrawal of FBS (Figure 5b). The observed increase in CCM3 expression was reversible after reintroduction of FBS into the cell culture medium (Figure 5c). To confirm the effect of serum deprivation on CCM3 transcription, cultures were exposed to the transcription inhibitor actinomycin D. Actinomycin D inhibited the transcription, and therefore translation, of CCM3 (Figure 5d).

Given the known effect of CCM1/CCM2 signaling on the MAP kinase/p38 pathway, our group investigated how serum deprivation effected p38 activation. Serum deprivation increased the abundance of phosphorylated p38. The increase of phosphorylated p38 preceded the increase in CCM3 expression and also cleaved caspase-3 (Figure 5e).

PDCD10 siRNA decreases cell death

Under the FBS deprivation conditions described above, HUVECs were exposed to PDCD10 siRNA. Inhibition of PDCD10 led to decreased TUNEL positivity which reached statistical significance at 3 hours (Figure 6a). PDCD10 siRNA also led to muting of the increased level of cleaved caspase-3 seen under serum deprivation (Figure 6b). Additionally, PDCD10 siRNA conditions led to an attenuated increase in p38 expression (Figure 6c). This data further implicates CCM3 in the CCM1/CCM2 signaling pathway.

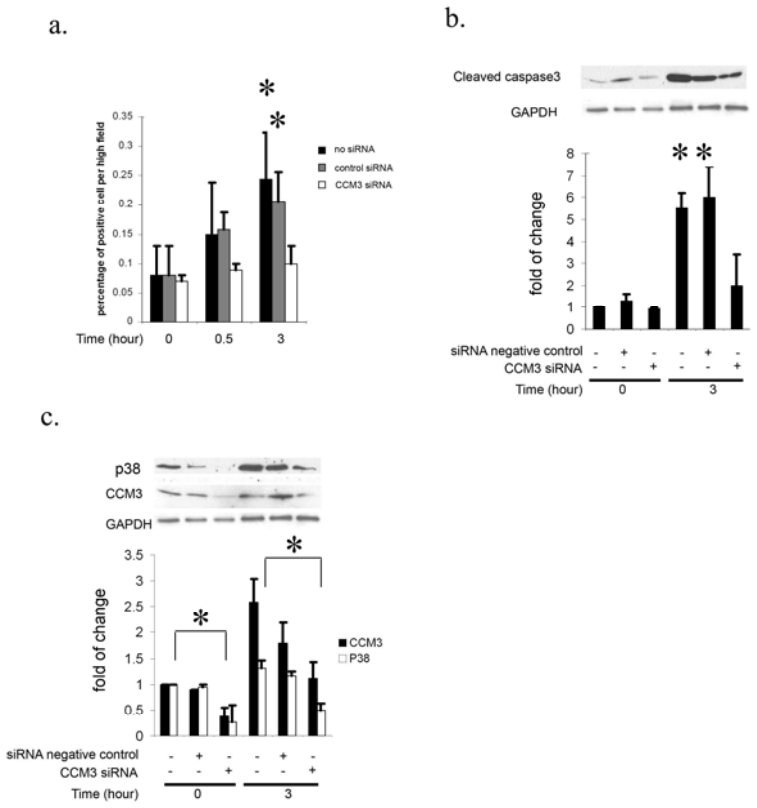

Figure 6 siRNA inhibition of CCM3/PDCD10 expression results in decreased cell death, p38, and activated Caspase-3 expression. *Courtesy of Leiling Chen MD and Murat Gunel MD*. (a) HUVECs treated with PDCD10 siRNA demonstrate decreased p38 expression levels compared to controls. (b) Serum-deprived HUVECs treated with PDCD10 siRNA show decreased apoptosis. (c) Serum-starved HUVECs show decreased activated caspase 3 levels after treatment with PDCD10 siRNA.

The above in vitro experiments provide strong evidence of CCM3's role in apoptosis. Overexpression of CCM3 led to increased morphological changes consistent with apoptosis, as well as, increased expression of the pro-apoptotic gene caspases-3. Serum deprivation experiments led to increased expression of CCM3, p38 and cleaved caspase-3. PDCD10 siRNA experiments led to an attenuation of the pro-apoptotic response. These results suggest that PDCD10 acts as a regulator of apoptosis. Specifically, PDCD10 expression promotes apoptosis. PDCD10 may act as in a tumor-suppressor like manner. Loss of PDCD10 function may lead to decreased apoptosis in vivo.

GFAP-Cre;CCM3$^{lox/lox}$ mice exhibit multiple developmental abnormalities

Mutant (GFAP-Cre;CCM3$^{lox/lox}$) mice are born according to the expected Mendelian ratio, although many fail to survive past weaning. Mutant mice weigh less and possess smaller bodies than littermate control animals, but have larger brains (Table 1). Mutant mice display severe ataxia, often moving in a circle.

Expression of CCM3 mRNA, as measured by in situ hybridization, is reduced in the mutant CNS. Expression was not completely ablated and is expected to be unperturbed in the endothelium and most neurons (Figure 7).

	Body Weight (BoW)	% control	Brain Weight (BrW)	% control	BrW/BoW
P18 Control	5.3		0.34		
Experimental	4.28	80.75	0.42	123.53	1.53
P22 Control	10.24		0.45		
Experimental	4.37	42.68	0.52	115.56	2.71

Table 1 Analysis of *GFAP-Cre;Ccm3$^{lox/lox}$* animals reveals small body size but enlarged brain. Brain weight when corrected for body weight is 1.5-2.7 times that of control littermates. *Courtesy of Angeliki Louvi PhD and Murat Gunel MD*

Expression of GFAP is increased throughout the mutant CNS (Figure 8). The increase in GFAP expression could be a product of increased proliferation of GFAP expressing cells or a decrease in apoptosis present in the early development of the CNS. The large axon tracts of the corpus callosum are substantially thinner in the mutant brain. This result is evident upon sectioning, as well as, MRI and represents either a perturbation of myelination or a perturbation of axonal migration (Figures 8 and 9). Enlarged CNS vasculature was a finding which was observable by MRI and sectioning (Figures 9 and 10). Cerebrovascular capillaries, identified through in situ hybridization, were disorganized compared to control CNS, often lacking a vertical orientation (Figure 11). Analysis of the cerebellum through immunohistochemistry with antibodies against neurofilament

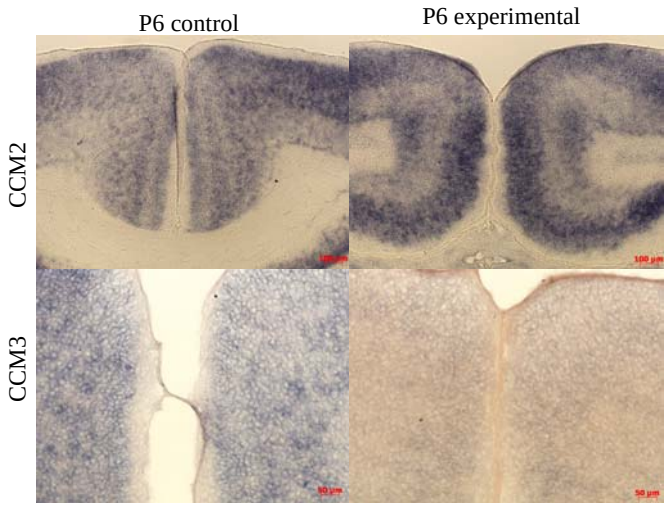

Figure 7 *Ccm3* mRNA (lower panel), is significantly downregulated in the brains of GFAP-Cre; *Ccm3*$^{lox/lox}$ animals (lower right). As a control, we evaluated *Ccm2* mRNA in both experimental and control animals as well and found it be unaltered (upper panels). *Courtesy of Angeliki Louvi PhD and Murat Gunel MD*

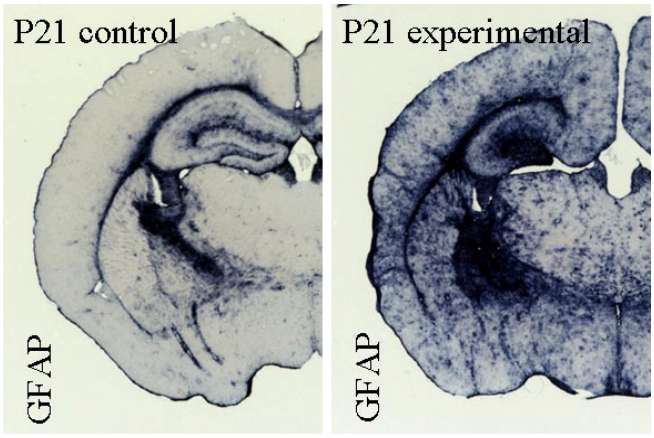

Figure 8 GFAP staining of GFAPCre;PDCD10-/- mouse (right panel) at P21 as compared to controls (left panel) reveal increased glial cell numbers and brain mass in the experimental animals. *Courtesy of Angeliki Louvi PhD and Murat Gunel MD*

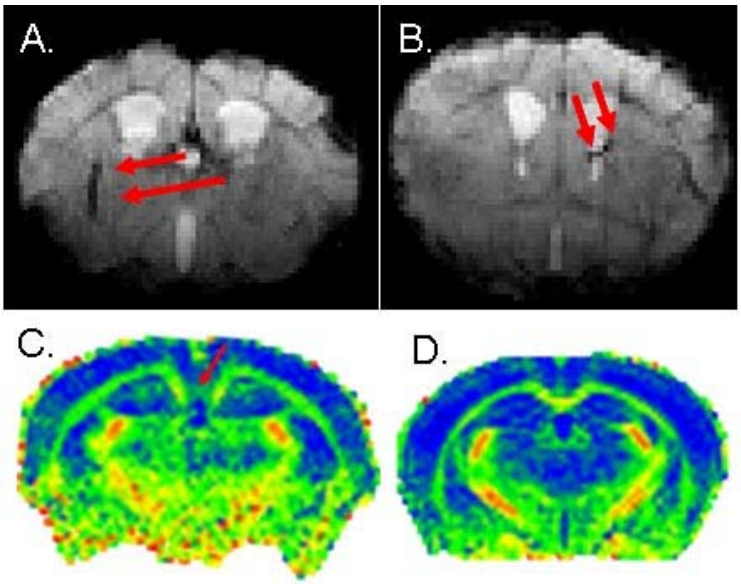

Figure 9 MRI imaging of a live 8 month *GFAP-Cre;Ccm3*$^{lox/lox}$ mice reveals enlarged vessels (red arrows) in A. and B. Interestingly, fractional anisotrophy detects thinner while matter in corpus callosum in experimental animal (red arrow) compared to a littermate D. Please note the larger brain size of the mutant in C. as compared to D. *Courtesy of Murat Gunel MD*

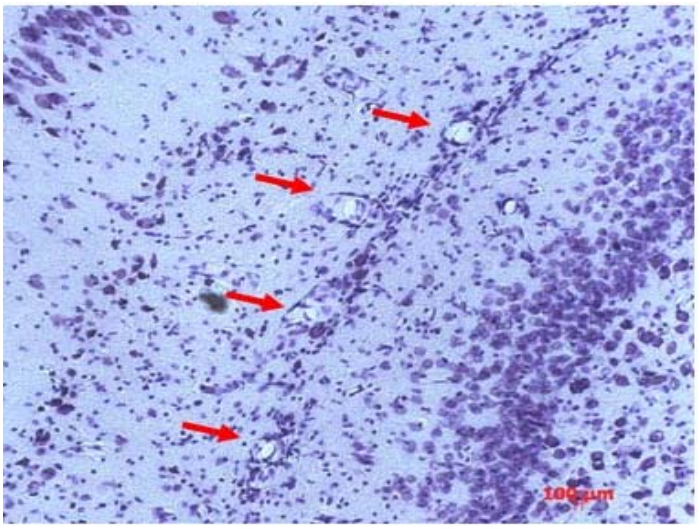

Figure 10 Histological examination of the brain of the *GFAP-Cre;Ccm3*$^{lox/lox}$ mutants reveal enlarged vessels (red arrows). *Courtesy of Angeliki Louvi PhD and Murat Gunel MD*

revealed a lack of Purkinje cell monolayers, possibly accounting for the problems with gait observed in mutant mice (Figure 12).

Most GFAP-Cre;CCM3$^{lox/lox}$ mice do not survive past weaning. Analysis of five mutants which survived past weaning revealed a persistent weight discrepancy between mutant and control, with the mutants weighing on average 80% that of the control mice. One adult mutant presented with two superficial vascular malformations one near the olfactory bulb and the other near the pons (Figure 13). These malformations are very similar to lesions present in patients with CCM. MRI performed on two additional adult mutants revealed the presence of dilated vasculature, a finding common in human CCM (Figure 9).

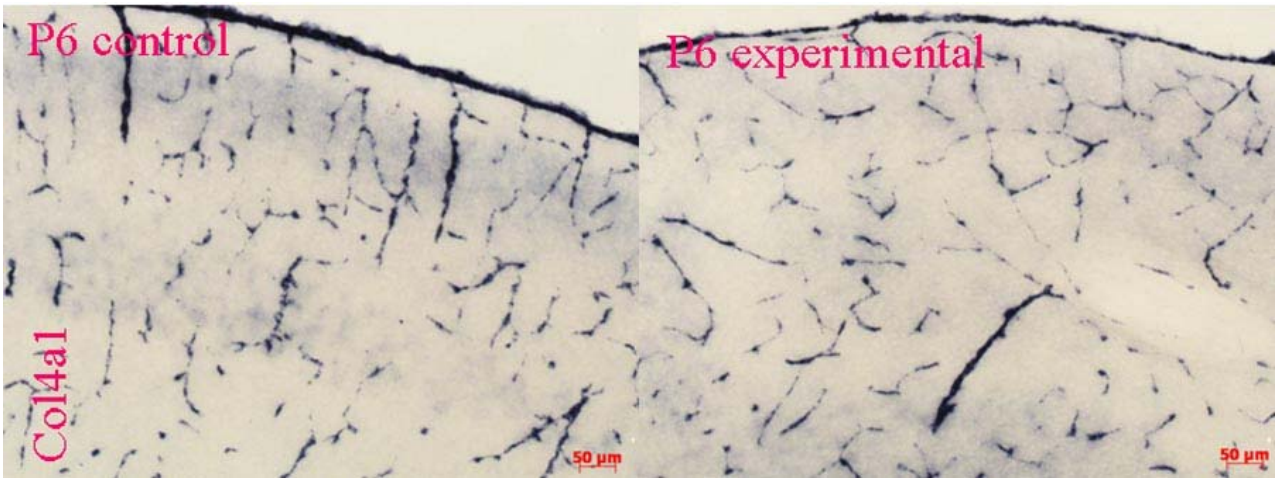

Figure 11 The organization of the cerebrovascular capillaries appear less orderly in the experimental animals (right panel) at P6 compared to controls (left panel) based on Col4a1 in-situ hybridization. *Courtesy of Angeliki Louvi PhD and Murat Gunel MD*

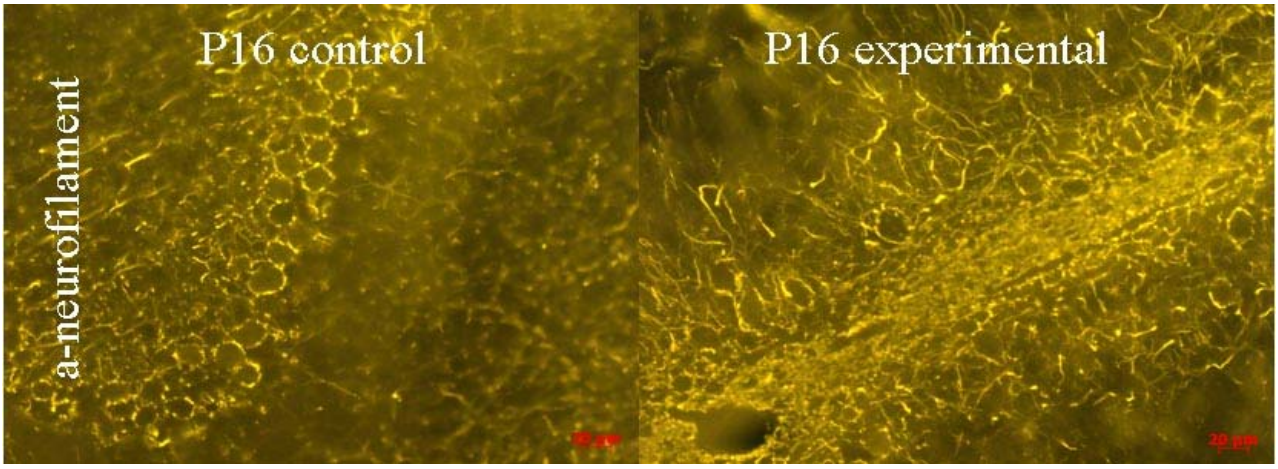

Figure 12 Purkinje cells are disorganized and appeared supernumerous in the cerebellum of the P16 experimental animals (right panel) as compared to controls (left panel) and as shown by axonal staining with neurofilament fluorescence. *Courtesy of Angeliki Louvi PhD and Murat Gunel MD*

Deletion of CCM3 effects proliferation and apoptosis in primary astrocyte culture

Astrocytes were isolated from GFAP-Cre;CCM3$^{lox/lox}$ and GFAP-Cre;CCM3$^{lox/+}$ mice as described below. Cells were plated at equal concentrations and allowed to grow in culture for 1, 2, and 3 days. Proliferation was measured by 3-(4,5-Dimethylthiazol-2-yl)-2,5-diphenyltetrazolium bromide (MTT, a tetrazolium salt) assay on each day. Reduction of the tetrazolium salt in the mitochondria can be measured using a

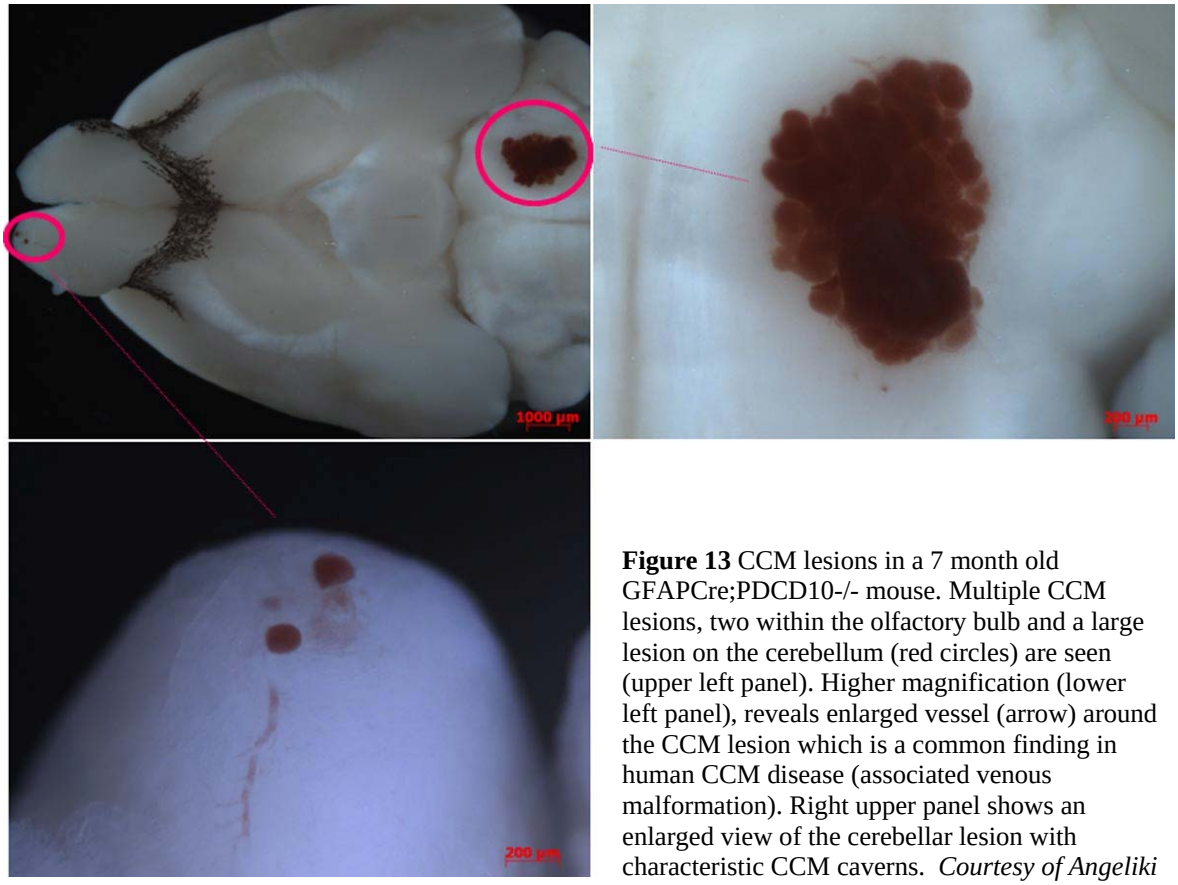

Figure 13 CCM lesions in a 7 month old GFAPCre;PDCD10-/- mouse. Multiple CCM lesions, two within the olfactory bulb and a large lesion on the cerebellum (red circles) are seen (upper left panel). Higher magnification (lower left panel), reveals enlarged vessel (arrow) around the CCM lesion which is a common finding in human CCM disease (associated venous malformation). Right upper panel shows an enlarged view of the cerebellar lesion with characteristic CCM caverns. *Courtesy of Angeliki Louvi PhD and Murat Gunel MD*

spectrophotometer and correlates to the number of viable cells in culture. GFAP-Cre;CCM3$^{lox/lox}$ cultures displayed a growth advantage at day 1, which persisted through day 3 (Figure 14).

The increased MTT signal in the GFAP-Cre;CCM3$^{lox/lox}$ cultures could be explained by decreased apoptosis, increased proliferation or both. To further elucidate life cycle changes, cultures were analyzed by immunohistochemistry using antibodies against Ki67, a known marker of proliferation. GFAP-Cre;CCM3$^{lox/lox}$ cultures exhibited increased proliferation within 24 hours as compared to GFAP-Cre;CCM3$^{lox/+}$ cultures (Figure 15). This result was confirmed by BrdU assays (Figure 16).

Next, our group exposed primary astrocytes to cycloheximide, a known inducer of apoptosis. GFAP-Cre;CCM3$^{lox/lox}$ cultures did not undergo apoptosis as GFAP-

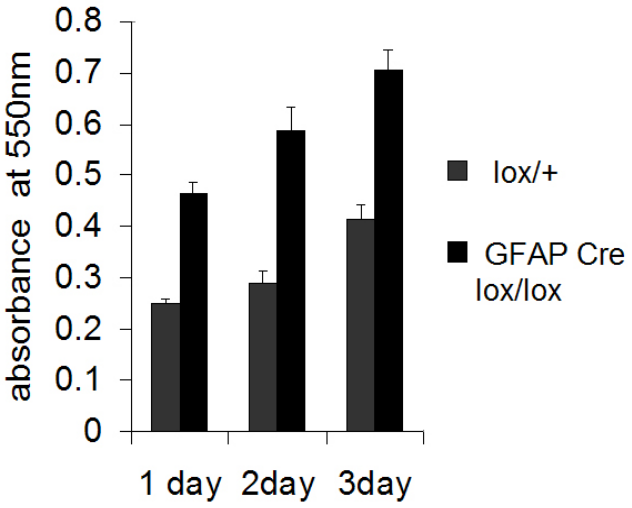

Figure 14 CCM3 deletion induced increase in proliferation was evaluated with MTT assay. Astrocytes were seeded at $1 \times 10^2/cm^2$ on poly-L-ornithine coated 96 well plates. The cells were allowed to attach overnight. At different time point (day 1, 3, 5), add 20 ul of MTT solution (5mg/ml) to each well containing cells. The absorbance was read at 550nm. *Courtesy of Leiling Chen MD and Murat Gunel MD*

Cre;CCM3$^{lox/+}$ cultures, as measured by TUNEL (Figure 17). Additionally, cycloheximide induced an increase of cleaved caspase-3 in the GFAP-Cre;CCM3$^{lox/+}$ culture. This effect was attenuated in the GFAP-Cre;CCM3$^{lox/lox}$ culture (Figure 18).

Deletion of CCM3 effects integrin dependent cell function

Beta-1 integrin's role in cell adhesion and migration is well established [42], [43] [44], [45]. Cell migration was tested by allowing cultures to grow to confluence then scratching the culture dish with a pipette tip. Migration through the cell free zone was stunted in the GFAP-Cre;CCM3$^{lox/lox}$ cultures and continued to trail the GFAP-Cre;CCM3$^{lox/+}$ cultures through 48 hours (Figure 19).

Cell adhesion was tested using three different substrates (Figure 20). Neither culture adhered well to vitronectin. Both GFAP-Cre;CCM3$^{lox/lox}$ and GFAP-Cre;CCM3$^{lox/+}$ cultures exhibited a higher affinity to the beta-1 integrin substrates, fibronectin and laminin. Although the GFAP-Cre;CCM3$^{lox/lox}$ cells tended not adhere as well to beta-1 integrin substrates, the difference is insignificant. The question remains of how the GFAP-Cre;CCM3$^{lox/lox}$ cultures would compare to a wild-type control.

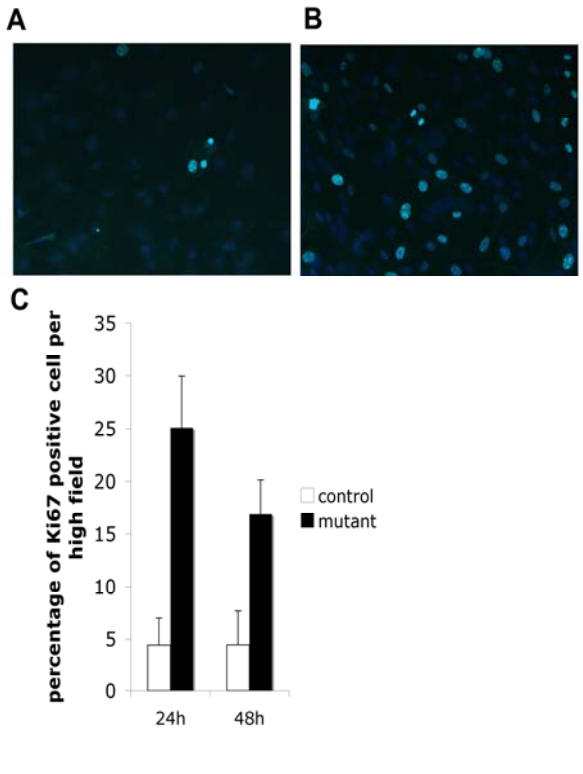

Figure 15 Alternatively, CCM3 deletion induced increase in proliferation was evaluated with ki67 immunohistochemistry staining: Astrocytes were seeded on poly-L-ornithine coated 4 well culture slides. At different time point, the cells were fixed in 4%PFA, and the percentage of positive ki67 per high field (x40) was count. The photo-imagine show the representative imagine for the ki67 immunostaining at 24 hours culture (x20). The positive ki67 is green and nuclear staining, the blue is DAPI counter staining. A. control astrocyte; B Mutant astrocyte; C. quantization of positive ki67 percentage. *Courtesy of Leiling Chen MD and Murat Gunel MD*

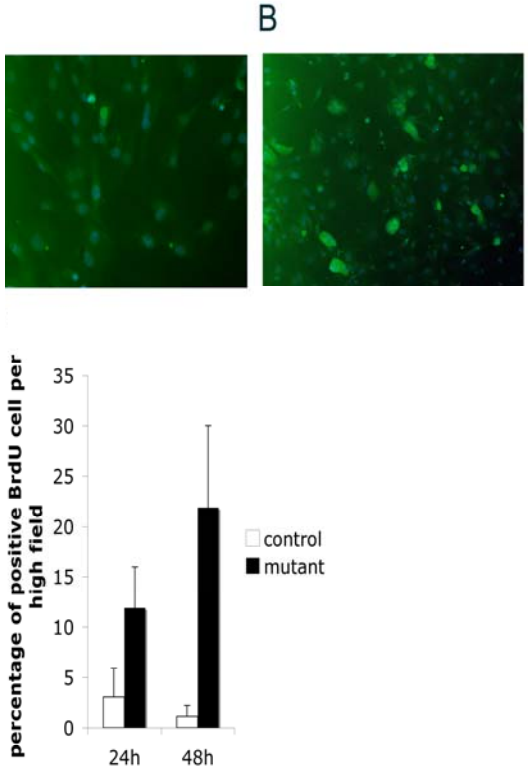

Figure 16 Furthermore, CCM3 deletion induced increase in proliferation was evaluated with BrdU incorporation assay: Astrocytes were seeded on poly-L-ornithine coated 4 well culture slides, and incubated with 10um BrdU. At different time point, the cells were fixed in 4%PFA, and the percentage of positive BrdU per high field (x40) was count. The photo-imagine show the representative imagine for the BrdU immunostaining at 24 hours culture (x20). The positive BrdU is green and nuclear staining, the blue is DAPI counter staining. A comes from control (GFAP Cre;lox/+); B comes from mutant (GFAP Cre; lox/lox). *Courtesy of Leiling Chen MD and Murat Gunel MD*

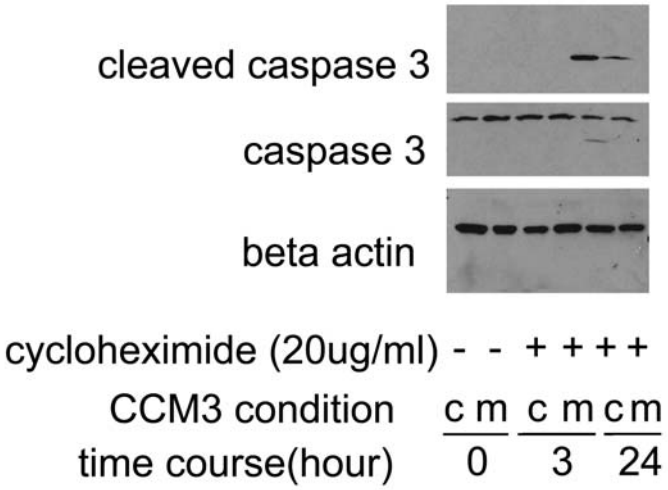

Figure 18 CCM3 deletion in astrocyte results in resistance of cycloheximide induced apoptosis: . Astrocytes were seeded at 2×10^5 on poly-L-ornithine coated 10cm plates, and incubated 48 hours, then 20ug/ml cycloheximide was added into medium. At different time point, cells were lysed, and followed with western blotting. *Courtesy of Leiling Chen MD and Murat Gunel MD*

Methods (performed by author)

Mouse Colony.

Experiments were carried out in accordance with protocols approved by the Institutional Animal Care and Use Committee at Yale University School of Medicine. Mouse colonies were maintained at Yale University, in compliance with National Institutes of Health guidelines and with the approval of Yale University Institutional Animal Care and Use Committee. To generate experimental animals, males with the genotype of *Promoter*-Cre;CCM3$^{lox/+}$ were mated with females lacking the Cre transgene and possessing a CCM3$^{lox/lox}$ genotype. For timed pregnancies, midday of the day of vaginal plug discovery was considered embryonic (e) day 0.5. Mice at embryonic and postnatal stages through adulthood were used. For embryonic stages, pregnant females were anesthetized and pups at appropriate stages were dissected from the uterus. Embryonic brains/neural tubes were dissected and fixed by immersion in 4% paraformaldehyde (PFA) in phosphate buffered saline (PBS) overnight. Mouse pups [postnatal (P) day 0 through P2] were anesthetized on ice, then the brains were removed and fixed in 4% PFA overnight. At all other stages, mice were anesthetized and intracardially perfused with 4% PFA.

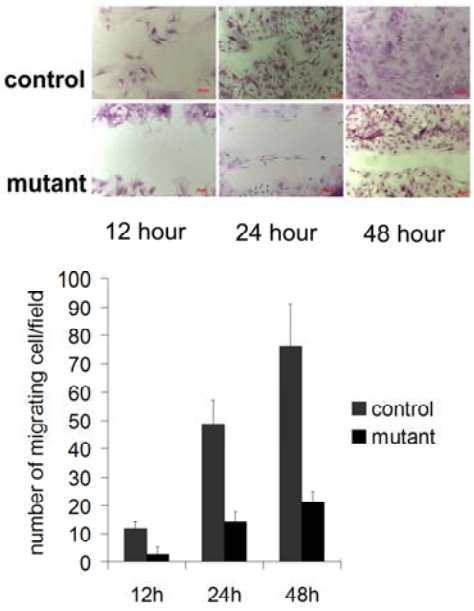

Figure 19 : Deletion of CCM3 results in Deletion decreased migration of astryocte. Astrocytes are plated in tissue culture dishes (10mg/ml poly-L-ornithine coated), and after 24 h of incubation, the confluent monolayer of cells was scratched in a standardized manner with a plastic tip to create a cell-free zone in each well, 2 mm in width. The medium was aspirated and replaced with DMEM/F12 plus 10% FBS. At desired time point, the cells were fixed in 4%PFA, and stained using 0.1%crystal violet. *In vitro* re-epithelialization was documented by photography. *Courtesy of Leiling Chen MD and Murat Gunel MD*

DNA Preparation from Mouse Tissue. Tissue was collected from the mouse for genotyping. For embryonic mouse stages the yolk sac was taken and for later stages (postnatal day 0 or older) a small portion of tail was taken. The tissue was combined with 90 µl of sterile water and incubated at 95°C for 10 minutes. The samples were briefly spun down and brought down to room temperature (2-3 minutes). 10 µl of proteinase K (at 2 µg per µl concentration) was added and mixed well. The samples were then incubated at 55°C overnight and then 95°C for 10 minutes to inactivate the proteinase K. After centrifugation the resulting supernatant was used for PCR analysis.

PCR. PCR was performed to genotype the transgenetic mouse lines used in this study. The standard reaction contained 10 µl 2x FailSafe^{TM} Buffer Premix F (Epicentre, Madison, WI), 0.3 µl of 10 µmol of each primer, 0.5 µl of DNA, and 0.2 µl of Taq DNA polymerase isolated from an E. coli strain that carries the DNA polymerase gene from T. aquaticus. The amplification protocol was comprised of a denaturation step at 95°C for 4

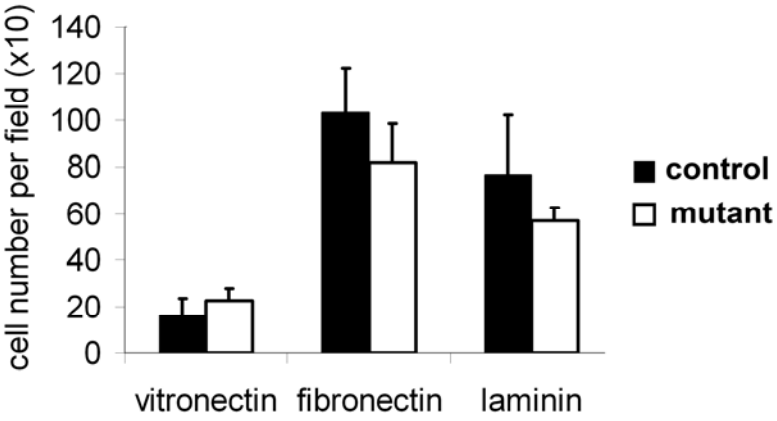

Figure 20 CCM3 deletion results in no change in adhesion of astrocye to extracellular matrix. Murine lamnin-1, bovine fibronectin, and bovine vitronectin will be obtained from Sigma. 10ug/ml of ECM solution is added on Petri dish 2 hous at 37ºC. Before addition of cells, all substractes were blocked with heat-inactivated bovine serum albumin to prevent non specific binding the substrates. After washed with PBS, the cells ($2x10^3$) added for 30 minutes. The adhesion assay is stopped by adding DMEM/F12 plus 10% FBS to the Petri dish and washed off loosely attached cells. The attached cells are then fixed with 4% paraformaldehyde in PBS for 20 minutes. Adhesion was quantified counting all attached cells under phase microscopy. *Courtesy of Leiling Chen MD and Murat Gunel MD*

min, followed by 35 cycles of a 95°C denaturation step for 30 sec, an annealing step at 55°C for 30 sec, and a 45 sec extension step at 72°C. The reaction was completed with a 10 min extension step at 72°C. The primers used to for genotyping were as follows: Cre primer 1, CCGGGCTGCCACGACCAA; Cre primer 2, GCGCGGCAACACCATTTTT, CCM3 primer 1, CTCAGTGTAGTCATGAAAAGAGT; CCM3 primer 2, CCAGCATCCTTTGCCTCTCC. The Cre primer set generated a 500 base pair product. The CCM3 primers resulted in a 150 base pair product for the knock-out genotype compared to a 103 base pair product for the wild-type genotype. PCR products were analyzed using gel electrophoresis.

Riboprobe synthesis for in situ hybridization. Templates for riboprobe synthesis were derived from cloned mouse cDNA sequences of the corresponding genes: *T-box brain gene 1* (*TBR1*), *Chick ovalbumin upstream transcription factor I* (*COUP-TFI*), *Calbindin* (*CALB*), *Pou Domain, class 3, transcription factor 1* (*SCIP*), *Ephrin A5, Notch,*

Retinoid-related orphan receptor alpha (*ROR*α), β*-tublin.* The constructs were previously made and consisted of the cDNA inserted 3' to 5' in respect to a T7 promoter in a plasmid DNA backbone. This design allows for an anti-sense RNA transcript to be synthesized utilizing T7 RNA polymerase and digoxigenin-11-UTP. Before RNA synthesis, plasmids were first linearized with a restriction enzyme digest. After digestion, the reaction was treated with 0.005% sodium dodecyl sulfate (SDS) and proteinase K (final concentration of 0.7 mg/ml) for 15 minutes at 37°C. The DNA templates were then purified using a phenol/chloroform/isoamyl alcohol extraction. Briefly, a phenol/chloroform/isoamyl solution (25 parts phenol to 24 parts chloroform to 1 part isoamyl alcohol) was added at an equal volume to the DNA sample. After inverting several times, the samples were spun down at 14,000 rpm for 5 minutes and the aqueous phase (top layer) was transferred to a new tube. An equal volume of chloroform/isoamyl alcohol (24 parts chloroform to 1 part isoamyl alcohol) was then added, mixed well, centrifuged down at 14,000 rpm for 5 minutes, and the aqueous layer was removed again. This last step was repeated once more. An ethanol precipitation of the DNA was then performed by adding 2.1 times the volume of 100% ethanol and 0.1 times the volume of 3 M sodium acetate. The DNA was incubated on ice for 15 minutes and spun down at 14,000 rpm for 15 minutes at 4°C. The supernatant was discarded and the pellet was washed with 70% ethanol and centrifuged at 14,000 rpm for 5 minutes. The pellet was allowed to dry and resuspended in 20 μl of DEPC-treated H_20. This linearized and purified DNA was then used as the template DNA for riboprobe transcription. The transcription reaction consisted of 1 μg of DNA, 2 μl of 10x transcription buffer, 2 μl of nucleotide mixture (containing digoxigenin-11-UTP), 1 μl RNase Inhibitor, 1 μl of 100

mM DTT, and 2 μl T7 RNA polymerase. The reaction was incubated at 37°C for 2 hours. 2 μl of DNase was then added and incubated for 15 minutes at 37°C. The RNA was precipitated by adding 100 μl of DEPC-treated H_20, 10 μl of lithium chloride and 300 μl of 100% ethanol and incubated on ice for 15 minutes. The RNA was pelleted by spinning at 14,000 rpm for 15 minutes at 4°C and washed once with 70% ethanol. After drying the pellet, the riboprobe was resuspended in 100 μl of DEPC-treated H_20 and checked for quality on an agarose gel.

***In situ hybridization*.** Mouse brains were post-fixed overnight in 30% sucrose/4% PFA and sectioned in the coronal plane on a Leica sledge cryomicrotome at 36 μm (Leica Microsystems, Germany). Sections were mounted on slides and allowed to dry overnight before further processing. For the *in situ* hybridization all incubation and wash steps were performed on a rocker when possible in RNase-free conditions. The slides were first treated with 4% PFA for 15 minutes and wash 3 times for 5 minutes each in DEPC-PBS. For mouse stages P0 through P20 the slides were incubated in detergent solution (consisting of) for two 15 minute intervals. For older stages, 30 minute incubation periods were used and no detergent treatment was used for embryonic tissue sections. After detergent treatment, the slides were washed once in DEPC-PBS and then incubated with proteinase K solution (at a concentration of 1.02 μg/ml) for 30 minutes at 37°C. Slides were fixed again in 4% PFA for 15 minutes and then washed three times 5 minutes in DEPC-PBS. Then the slides were pre-incubated in hybridization solution (consisting of) at 70°C for an hour. 70 μl of the prepared riboprobe (see above) was added to 14 ml of hybridization and mixed. Slides were incubated in the riboprobe solution overnight at

70°C. The following day slides were washed in a stringent wash (containing formaldehyde) three times for 45 minutes each at 70°C. Then three washes with Tris-buffered saline containing 0.1% Tween-20 (TBST) were performed. The slides were placed in blocking step in 10% lamb serum in TBST for 60 minutes prior to incubation with an alkaline phosphotase conjugated anti-DIG antibody (at a 1:5000 concentration in 1% lamb serum TBST) for 2 hours at room temperature. Three washes in TBST for 15 minutes were done before developing with 5-Bromo-4-Chloro-3'-Indolyphosphate p-Toluidine Salt (BCIP) and Nitro-Blue Tetrazolium Chloride (NBT). Development time differed depending on the riboprobe ranging from overnight to 2 days. Afterwards the slides were dehydrated in a series of ethanol steps, cleared with Histoclear (a xylene substitute) and cover-slipped. Sections were analyzed using a Zeiss Stemi dissecting microscope or a Zeiss AxioImager (Zeiss, Oberkochen, Germany) fitted with an AxioCam Mrc5 digital camera. Images were captured using AxioVision AC software (Zeiss) and assembled using Adobe Photoshop.

Nissl Stain. Mouse brains were perfused, prepared and sectioned as described above. 36μm sections on Fisherbrand Superfrost microscope slides were dried at room temperature (RT) overnight. Samples were placed in 4% PFA for 15 minutes on a rocker at RT. Next, samples were rinsed twice in PBS for 5 minutes each wash at RT. Samples were then soaked in distilled water (DW) for 1 minute. Samples were then exposed to an ethanol gradient for one minute in each: 70, 80, 90, 95, 100, 100%. Samples placed in xylene for 1 minute and then another xylene bath for 30 minutes. Samples were then transferred back to the first xylene bath for one minute and then down the ethanol

gradient, in each bath for one minute (100, 100, 95, 90, 80, 75). Samples were placed in DW for one minute. Next samples were incubated at 42^{o} C for 5 minutes in 0.1% Cresyl Violet in DW (previously filtered through 3mm filter paper). Samples were then washed in DW to remove excess stain. Samples then were exposed to acid ethanol (100% ethanol, trace acetic acid) for 5-10 minutes until contrast was appropriate. Samples were transferred to an ethanol gradient for one minute in each concentration (, 80, 90, 95, 100, 100%). Samples were then bathed in Histoclear 3 times for 1 minute each. Slides were then coverslipped with Eukitt. Sections were analyzed using a Zeiss Stemi dissecting microscope or a Zeiss AxioImager (Zeiss, Oberkochen, Germany) fitted with an AxioCam Mrc5 digital camera. Images were captured using AxioVision AC software (Zeiss) and assembled using Adobe Photoshop.

BrdU Assay. Pregnant mice were subjected to intraperitoneal injections of 5-bromo-2-deoxyuridine (BrdU) 20μg/g at appropriate embryonic time points measured by date of seminal plugging. For short course experiments, pregnant mice were sacrificed 3 hours after injection of BrdU. Embryos were dissected and fixed in 4% PFA for 2 hours. Long course experiments consisted of post-natal time points (P0 or P2). At these time points, mouse brains were perfused, prepared and sectioned as described above. Sections were mounted on slides and allowed to dry overnight before further processing. All incubation and wash steps were performed on a rocker when possible. The slides were first treated with 4% PFA for 15 minutes and wash 3 times for 5 minutes each in DEPC-PBS. For mouse stages P0 through P20 the slides were incubated in detergent solution (consisting of) for two 15 minute intervals. For older stages, 30 minute incubation periods were used

and no detergent treatment was used for embryonic tissue sections. After detergent treatment, the slides were washed once in DEPC-PBS and then incubated with proteinase K solution (at a concentration of 1.02 μg/ml) for 30 minutes at 37°C. Slides were fixed again in 4% PFA for 15 minutes and then washed three times 5 minutes in DEPC-PBS. Then the slides were pre-incubated in in-situ hybridization solution (without riboprobe) at 70°C overnight. Slides were washed in Solution X twice for 20 minutes each at 70°C. Two TBST washes were performed for 10 minutes each at RT. Slides were bathed in 2N HCL for 30 minutes at RT. Four washes in 100mM Tris-HCl (pH 8.5) for 5 minutes each were performed. Samples were then washed in TBST, three times, for 5 minutes each. Next slides were blocked in 10% lamb serum in TBST for 60 minutes at 4°C. Anti-BrdU antibodies were added to slides and placed at 4^{o}C overnight. Three washes in TBST for 15 minutes were done before incubating with anti-fluorophore antibody in 1% lamb serum overnight at 4^{o}C. Slides were washed three times in TBST then developed with 5-Bromo-4-Chloro-3'-Indolyphosphate p-Toluidine Salt (BCIP) and Nitro-Blue Tetrazolium Chloride (NBT). Afterwards the slides were dehydrated in a series of ethanol steps, cleared with Histoclear (a xylene substitute) and cover-slipped. Sections were analyzed using a Zeiss Stemi dissecting microscope or a Zeiss AxioImager (Zeiss, Oberkochen, Germany) fitted with an AxioCam Mrc5 digital camera. Images were captured using AxioVision AC software (Zeiss) and cells counted using ImageJ v1.38 software (NIH). Statistical analysis was not performed on these pilot experiments, but will be performed in the future.

Astrocyte Cultures. Primary astrocytes for FACS analysis were isolated and cultured from early post-natal mice (P0-P2) by Leiling Chen MD using an established protocol [46]. For the apoptosis experiments, astrocytes were exposed to media containing 20 mg/ml cycloheximide. Cells were harvested after 3 hours for FACS analysis.

HUVEC Cultures. Human umbilical vein endothelial cells (HUVECs) were obtained from the Vascular Biology and Transplantation Program at Yale University School of Medicine (New Haven, CT). HUVECs were grown on 0.1% gelatin coated 6-well plates using 20% fetal bovine serum (FBS), 1% endothelial cell growth supplement (ECGS) in M199. Media was changed every third day. Cells were used in experiments between passages 3-6. For experimental conditions, HUVECs were grown to confluence (~2 days in culture). Next, fresh media was supplemented with antibody to β1-integrin (P4C10 or TS2/16) or mouse IgG. Cells were harvested for western blotting after 72 hours of incubation.

Western Protocol. Cells were harvested and total protein from the cells was extracted in a lysis buffer (150mM NaCl, 1%Triton X-100, 0.5% sodium deoxycholate, 0.1% SDS, 50mM Tris-HCl pH 8.0 and protease inhibitors, 1mM Na_3V0_4, 10mg/ml leupeptin, 10mg/ml aprotinin and 4mM PMSF). Cell lysate was centrifuged, supernatant collected and stored at -80^{o}C. Equal amounts of protein (approximately 50 µg/lane) were loaded into a 4-15% gradient polyacrylamide gel, separated by electrophoresis (Bio-Rad Laboratories, CA) and transferred onto a PVDF membrane (Bio-Rad Laboratories, CA). The membranes were incubated with primary antibody (caspase 3 antibody or anti-β-

actin [Santa Cruz, CA]) overnight at 4^{o}C. HRP conjugated secondary antibodies were used for visualization.

Annexin/PI Fluorescence Activated Cell Sorting. Primary astrocyte cultures (GFAP-Cre;CCM3$^{lox/lox}$ and GFAP-Cre;CCM3$^{lox/+}$) were trypsinized and washed with PBS. Cells were resuspended in 100μl of Annexin V Incubation Reagent (R and D Systems, Minneapolis, MN) per 10^6 cells for 15 minutes in the dark. Cells were acquired using a FACSCalibur flow cytometer (BD Biosciences). Analysis was performed using WinMDI v2.9. The astrocyte population was identified by forward and side-scatter properties. A threshold for annexin staining was set using the FITC channel by observing unstained (control) populations. Likewise, propidium iodide fluorescence was measured by using the PE channel in unstained (control) populations. From this data, quadrants were set and data acquired. Statistical analysis was not performed on these pilot experiments, but will be performed in the future.

Results

Tie2cre

Cre recombinase mediated recombination of CCM3 loxP sites, under the control of the endothelial cell specific promoter Tie2 failed to produce viable offspring which were homozygous for the CCM3 lox allele (Tie2-Cre;CCM3$^{lox/lox)}$. Heterozygous pups, Tie2-Cre;CCM3$^{lox/+}$, were found in an expected Mendalian manner. Gestational sacrifices revealed viable Tie2-Cre;CCM3$^{lox/lox}$ embryos at e9.5. Analysis of intact yolk sacs revealed a difference in vascular development between mutants and controls (Figure

21 A and B). This phenotype was also present at e10.5 (Figure 21 E and F). At e9.5 and e10.5, mutants were readily distinguishable from control littermates, being smaller in size

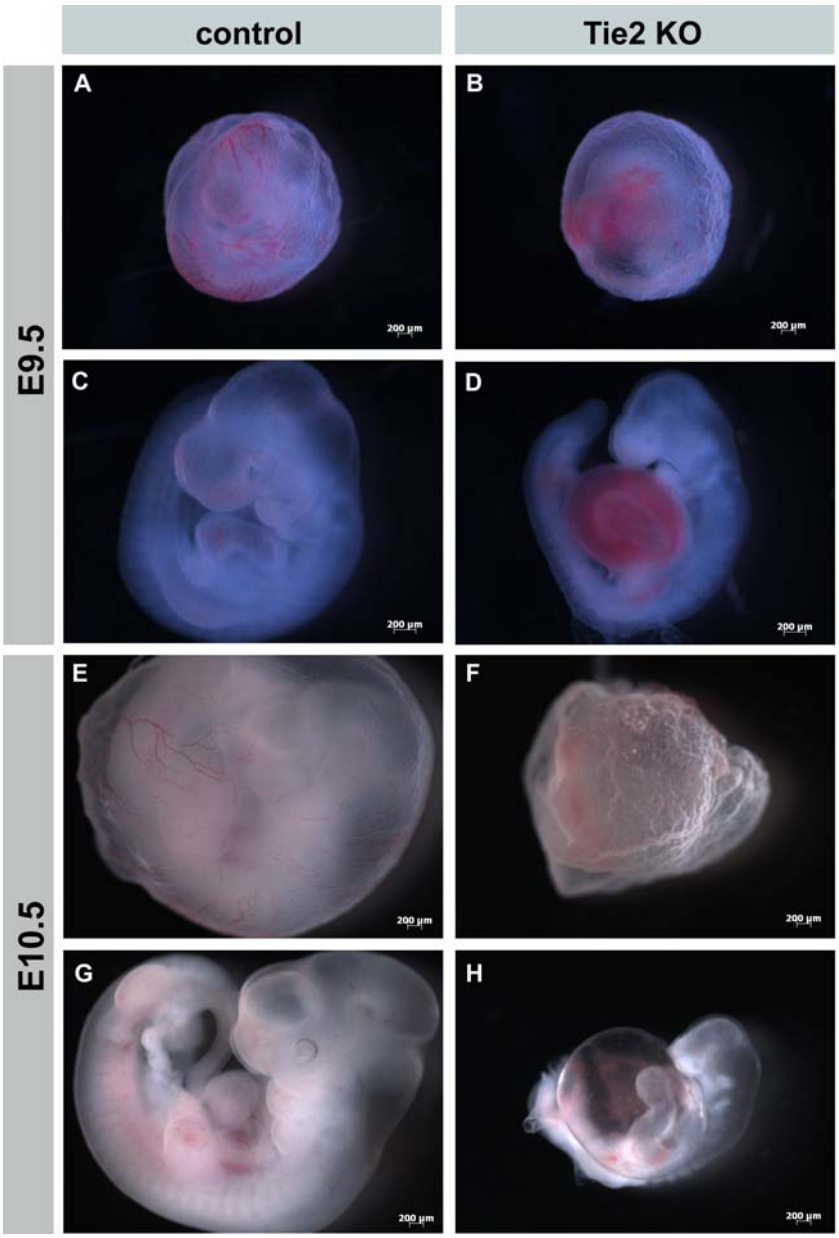

Figure 21 e9,5 and E10.5 Tie2-Cre;Ccm3$^{lox/lox}$ exhibit yolk sac and pericardial developmental abnormalities. E9.5 and E10.5 control yolk sacs display age appropriate vascular tree development (a and e). E9.5 and E10.5 Tie2 KO yolk sacs retain a primitive yolk sac consisting of islands of blood, lacking a vascular tree (b and f). E9.5 and E10.5 embryos exhibit a dilated pericardial region compared to controls (C, D, G and H).

and also containing a dilated cardiac region (Figure 21 C, D, G and H). A beating heart was present at e9.5, but was not observed at e10.5. No change in phenotype or developmental stage was apparent between e9.5 and e10.5 mutants.

Whole mount anti-PECAM staining revealed abnormal formation of the lower branchial arches (data not shown). India ink injected into the ventricle of e9.5 mutants

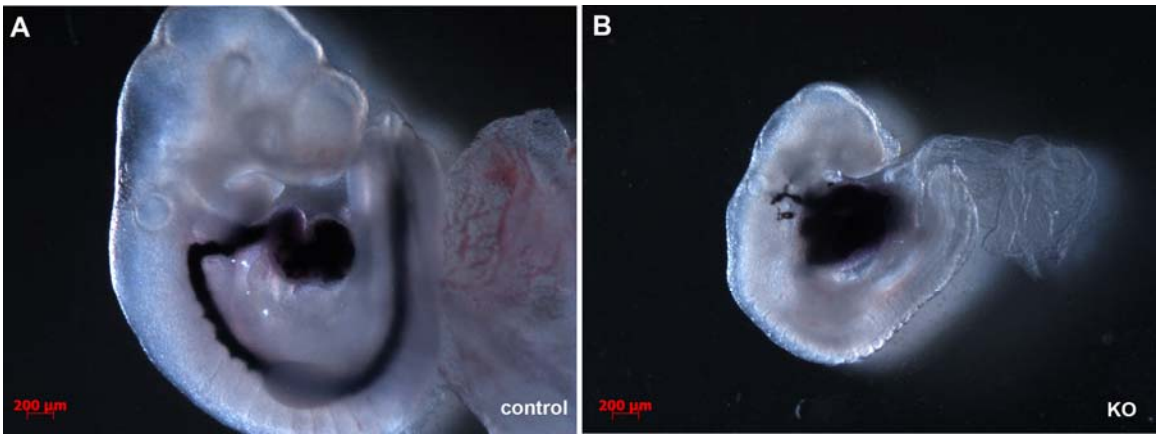

Figure 22 Tie2-Cre;Ccm3$^{lox/lox}$ embryos fail to develop normal vascular connections. Tie2-Cre;Ccm3$^{lox/lox}$ E9.5 embryos (b) injected with India ink into the primitive ventricle did not diffuse out of the heart, through the branchial arteries and down the dorsal aorta as littermate controls (a).

failed to travel through the distal caudal aorta (Figure 22). India ink mostly accumulated in the pericardial region in Tie2-Cre;CCM3$^{lox/lox}$ embryos. Some ink traveled into branchial arteries 2 and 3, although these arteries appeared constricted compared to control embryos. Dorsal aortae proximal to the heart were not easily identified in hematoxilin and eosin stained sections of e9.5 mutant embryos, but were readily identified in control embryos (Figure 23 A and C). Immunoflourescence of PECAM revealed the presence of endothelial cells, although the lumen lacked normal patency (Figure 23 B and D).

GFAPcre

Cre mediated recombination of CCM3 lox sites under the control of the GFAP promoter produced viable mutant mice at a frequency lower than the expected Mendelian ratio. GFAP-Cre;CCM3$^{lox/lox}$ pups can be phenotypically identified by gait abnormalities, small body habitus and a larger, rounder cranium (data not shown). Repeat polymerase chain reaction on phenotypically similar littermates revealed that there are a few GFAP-Cre;CCM3$^{lox/+}$ mice heterozygous for the lox allele which display a dysmorphic

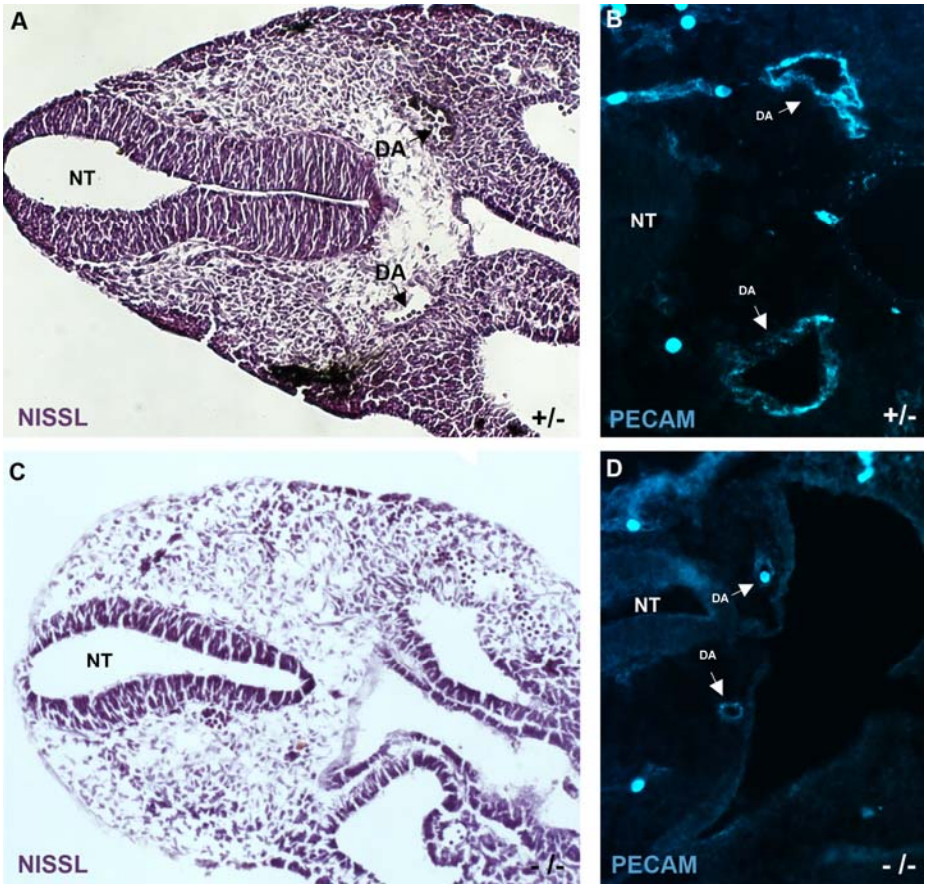

Figure 23 Tie2-Cre;Ccm3$^{lox/lox}$ embryos display abnormal dorsal aortae. H and E staining of E9.5 cross sections revealed an apparent lack of doral aortae in the Tie2-Cre;Ccm3$^{lox/lox}$ embryos (a and c). Subsequent immunohistochemistry with PECAM revealed the presence of endothelium and dorsal aorta with a significantly smaller lumen in the Tie2-Cre;Ccm3$^{lox/lox}$ embryos (b and d). NT = Neural Tube, DA = Dorsal Aorta

appearance, but not as severe as mutants. These littermates do not seem to have the gait abnormalities seen in the mutants.

Nissl staining of coronal sections revealed generalized disorganization of the cortical layers, hippocampus (including a smaller dentate gyrus) and cerebellum (Figure 24). In situ hybridization assaying known markers of cortical layering suggest a perturbation in neuron migration from the deeper layers to the more superficial layers of the cortex (Figure 25).

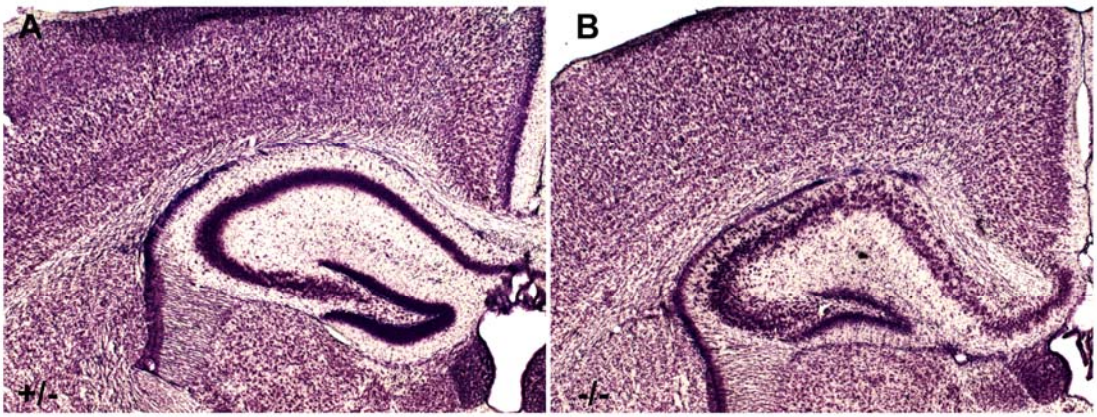

Figure 24 Nissl staining reveals abnormal cytoarchitecture. Adult GFAP-Cre;Ccm3$^{lox/lox}$ (b) exhibit generalized disorganization of cortical layers compared to control mice (a). Development of the hippocampus is perturbed; GFAP-Cre;Ccm3$^{lox/lox}$ mice displayed abnormal layering and a smaller dentate gyrus.

BrdU assays on cortical sections of embryonic day 14.5 embryos performed 3hr after injection of BrdU revealed decreased BrdU staining in cortical areas, excluding the ventricular layer (Figure 26). At e16.5, GFAP-Cre;CCM3$^{lox/lox}$ mice exhibited less BrdU uptake in layers of the somatosensory cortex above the ventricular zone and the basal ganglia (Figure 27). This trend was not observed in the visual cortex.

GFAP-Cre;CCM3$^{lox/lox}$ Astrocyte Culture

Astrocyte cultures isolated from postnatal day 1 GFAP-Cre;CCM3$^{lox/lox}$ mice and GFAP-Cre;CCM3$^{lox/+}$ mice exposed to cycloheximide and assayed by annexin-PI fluorescence activated cell sorting revealed a trend towards resistance to apoptosis in the mutant cultures (Figure 28).

Activation of β-1 integrin increase caspase-3 expression

The ability of antibodies to activate and block beta-1 integrin function was tested in our HUVEC culture conditions. Interestingly, P4C10, an antibody known to block

beta-1 integrin signaling [47], [37] decreased expression of caspase-3, as compared to control cultures. Conversely, TS2/16, an antibody known to promote beta-1 integrin signaling [48], slightly increased expression of caspase-3 (Figure 29).

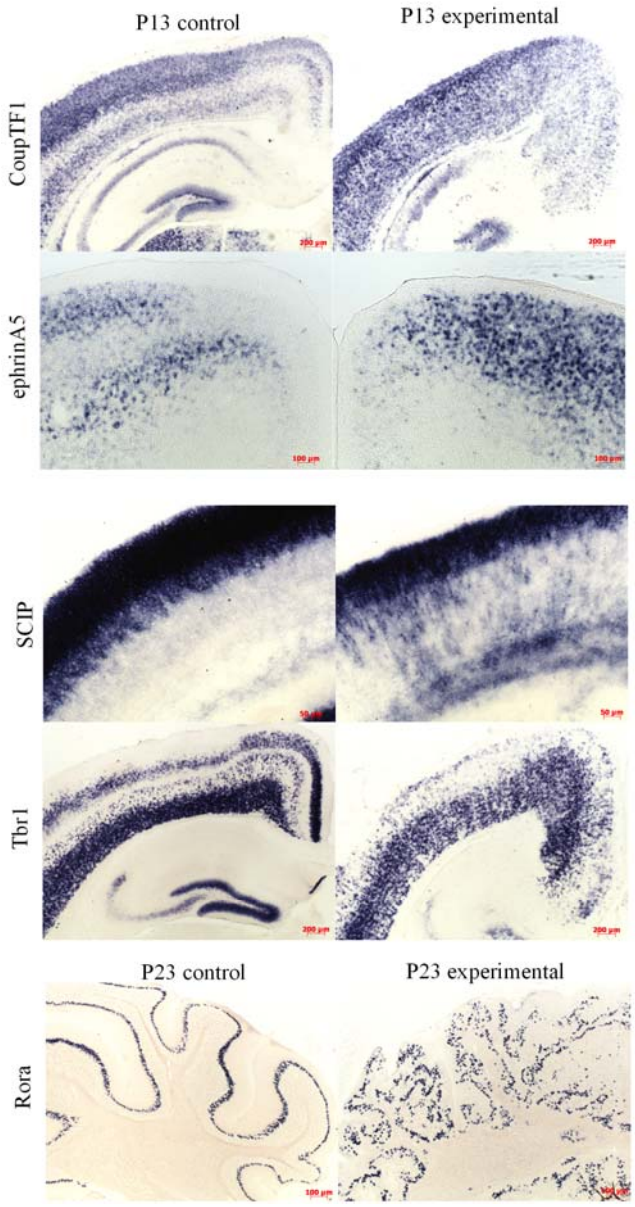

Figure 25 In situ hybridization on GFAP-Cre;Ccm3$^{lox/lox}$ sections exhibit abnormal development of cerebral cortical and cerebellar layers. Tbr1, SCIP, ephrinA5, CoupTF1 anti-sense probes were used to observe the development of cortical layers. Ror-α was used to analyze the cerebellum. GFAP-Cre;Ccm3$^{lox/lox}$ (right column) do not develop normal cortical layers as seen in control mice (left column).

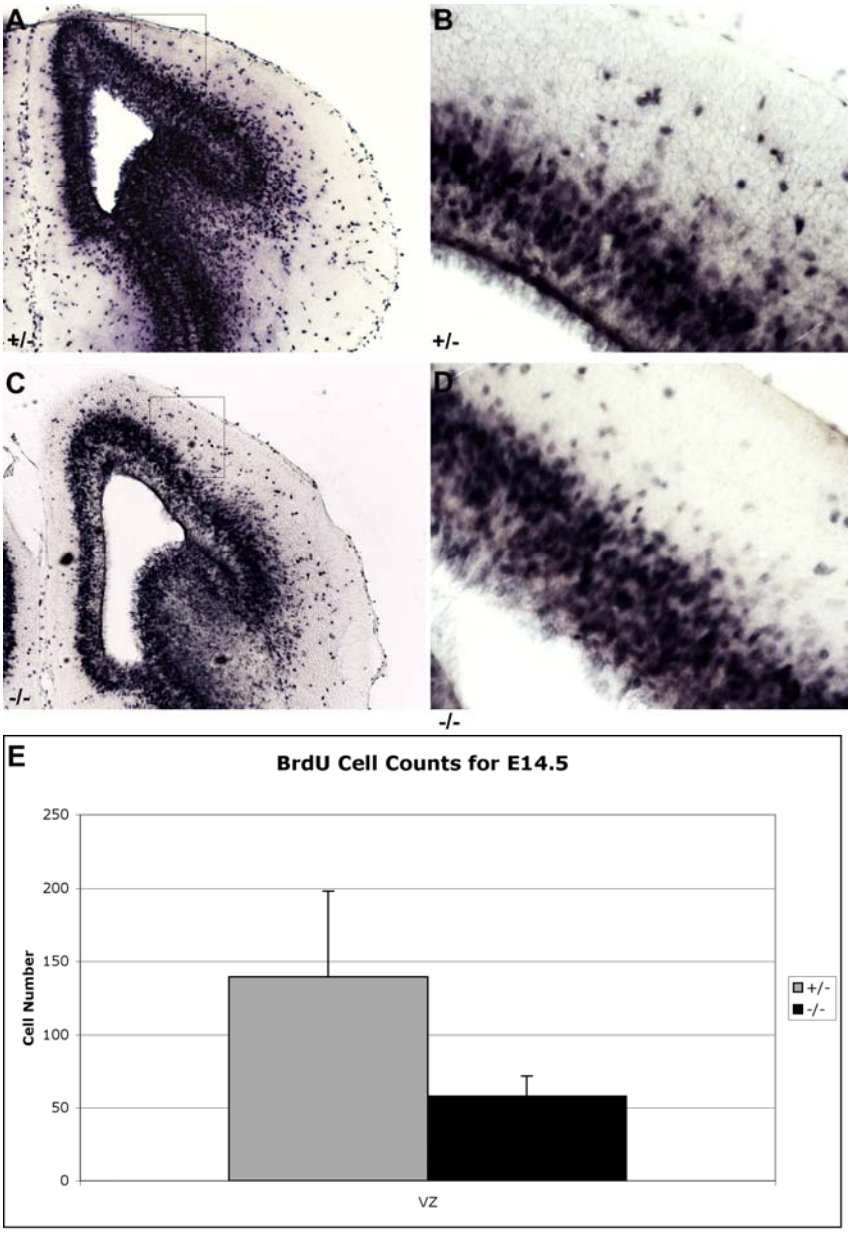

Figure 26 Three hour BrdU incorporation differs between GFAP-Cre;Ccm3$^{lox/lox}$ and GFAP-Cre;Ccm3$^{lox/lox}$ mice. GFAP-Cre;Ccm3$^{lox/lox}$ cortical sections (-/-, C and D) exhibit less BrdU incorporation compared to GFAP-Cre;Ccm3$^{lox/l+}$ cortical sections (+/-, A and B). Quantification was achieved with Image J software (E).

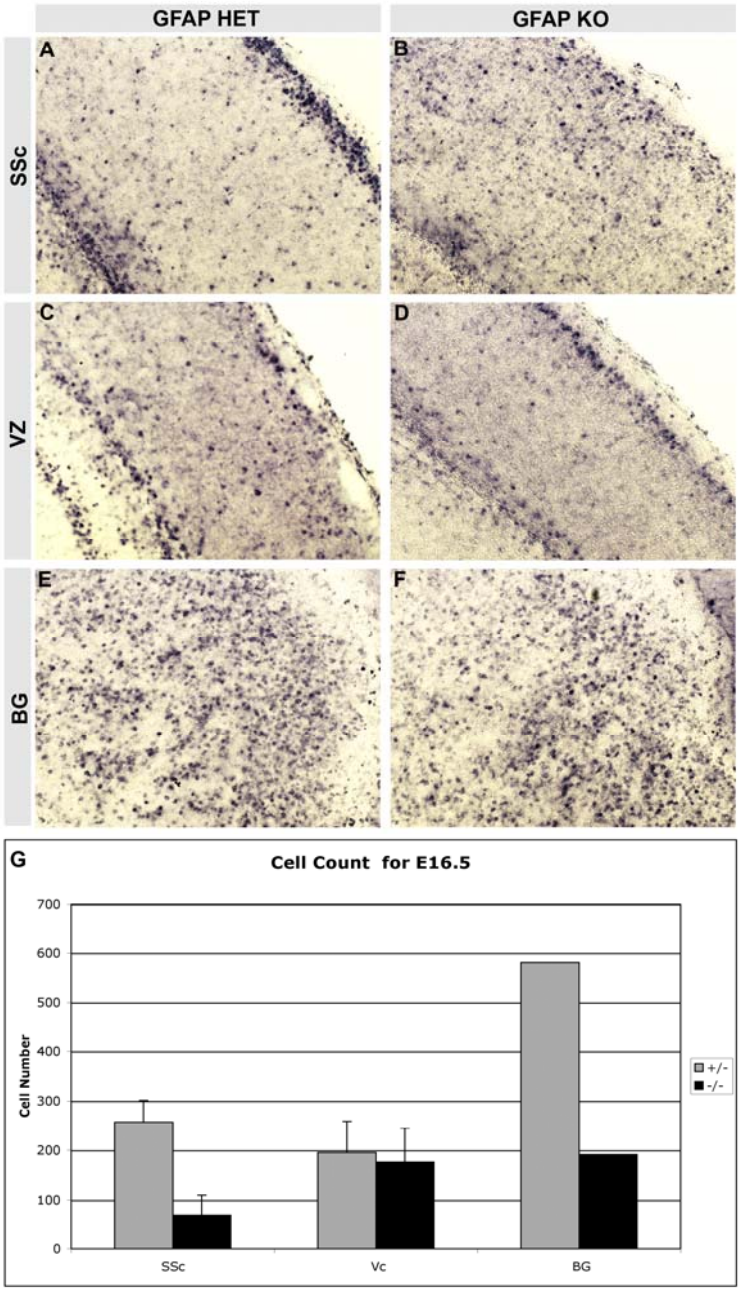

Figure 27 GFAP-Cre;Ccm3$^{lox/lox}$ and GFAP-Cre;Ccm3$^{lox/+}$ mice differ in the number of dividing cells present in the somatosensory cortex and basal ganglia. BrdU injections were performed at E16.5. Mice were sacrificed and assayed for BrdU incorporation at P2. GFAP-Cre;Ccm3$^{lox/lox}$ brains displayed less BrdU incorporation in the somatosensory cortex than GFAP-Cre;Ccm3$^{lox/+}$ brains (A and B). This finding was not obvious in the visual cortex (C and D). GFAP-Cre;Ccm3$^{lox/lox}$ also exhibited less BrdU incorporation in the basal ganglia (E and F). BrdU positive cells were quantified using Image J software (G). GFAP Het = GFAP-Cre;Ccm3$^{lox/+}$, GFAP KO = GFAP-Cre;Ccm3$^{lox/lox}$, Ssc = somatosensory cortex, Vc = visual cortex, BG = basal ganglia, +/- = GFAP-Cre;Ccm3$^{lox/+}$, -/- = GFAP-Cre;Ccm3$^{lox/lox}$

Discussion

Mice deficient in endothelial cell CCM3 are similar to CCM1 knockouts

Endothelial cell specific knockouts of CCM3 developmentally arrested around e9.5, one day after activation of the Tie2 promoter. Phenotypically, these mice resembled CCM1 homozygous knockout mice. Specifically, both CCM1 homozygous knock-outs and endothelial cell specific CCM3 knock-outs possess yolk sacs which lack a normal vascular tree, exhibit developmental arrest at e9.5, develop an enlarged pericardial region with hemorrhage, abnormal branchial arch development and lack normal dorsal aorta patency proximal to the heart [49]. In addition to the above findings, the CCM1 knock-out mice possessed dilated atria,

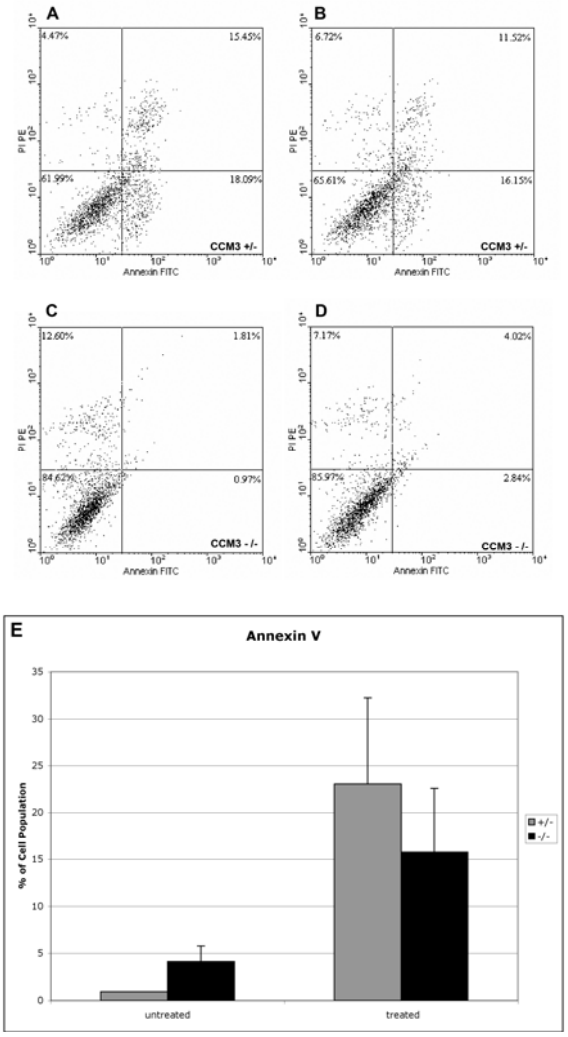

Figure 28 Primary astrocyte culture of GFAP-Cre;Ccm3$^{lox/lox}$ brains were resistant to cycloheximide induced apoptosis. Primary astrocyte cultures were exposed to cycloheximide (20μg/ml) for 3 hrs. Cells were analysed for apoptosis by staining for Annexin V. Flow cytometric analysis revealed fewer GFAP-Cre;Ccm3$^{lox/lox}$ astrocytes (C and D) entering apoptosis after 3 hrs exposure to cycoheximide compared to GFAP-Cre;Ccm3$^{lox/+}$ astrocytes (A and B). Quantification of 13 primary astrocyte cultures (6 GFAP-Cre;Ccm3$^{lox/lox}$ and 7 GFAP-Cre;Ccm3$^{lox/+}$) lacked significance, but a trend was present between GFAP-Cre;Ccm3$^{lox/lox}$ and GFAP-Cre;Ccm3$^{lox/+}$ cultures which underwent treatment with cycloheximide (E). CCM3 +/- = GFAP-Cre;Ccm3$^{lox/+}$, CCM3 -/- = GFAP-Cre;Ccm3$^{lox/lox}$, +/- = GFAP-Cre;Ccm3$^{lox/+}$, -/- = GFAP-Cre;Ccm3$^{lox/lox}$, untreated = no cycloheximide added to media, treated = media with cycloheximide

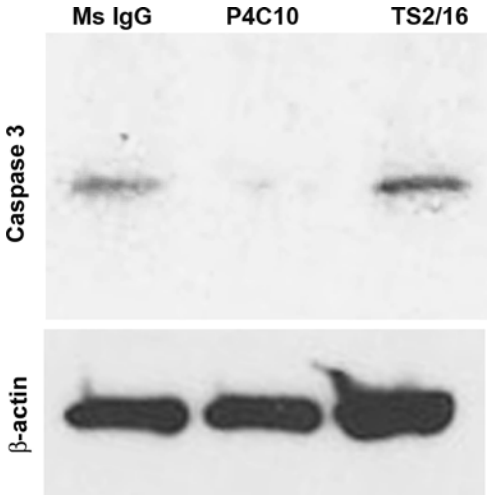

Figure 29 A blocker of β1-integrin signaling cascade attenuated expression of Caspase-3. HUVECs were cultured and allowed to grow to confluence. Western blot analysis was performed on cultures after a 3 day exposure to a β1-integrin activating antibody (TS2/16), a β1-integrin blocking antibody (P4C10) and a Mouse IgG control. The β1-integrin blocking antibody (middle lane) significantly reduced the expression of Caspase-3.

cranial vessels and caudal dorsal aorta. Quantification of mitotic endothelial cells in dilated vessels revealed increased endothelial cell proliferation in dilated vasculature. CCM1 knock-out embryos lacked normal expression of alpha-smooth muscle actin, an arterial marker. Furthermore, immunohistochemical analysis of CCM1 knock-out mice revealed decreased vascular expression of NOTCH4, which corresponds to human CCM [49]. This data further supports the hypothesis that CCM1 and CCM3 share a common molecular pathway as suggested by the similar phenotype in human CCM. Unfortunately, the phenotype alone does not prove CCM3 involvement in the CCM1 pathway. Knock-out mice of other genes important in vasculogenesis develop similar phenotypes. Loss of function mutations in activin receptor-like kinase-1 (ACVRL1) are known to cause hereditary hemorrhagic telangectasia. Murine knock-outs of ACVRL1 arrest at e9.5, lack an appropriate yolk sac vascular tree, display a dilated cardiac region, possess dilated cardinal veins and are deficient of the arterial-specific marker Efnb2 [50]. A mouse knock-out of vascular endothelial cell protein tyrosine phosphatase, a modulator of Tie2, display arrested development at e9.5, exhibit primitive yolk sac development (lacking a vascular tree), are significantly smaller than control embryos, develop pericardial edema, and exhibit collapsed dorsal aorta [51]. This data

raises the question of whether the phenotype our group has found is a common phenotype when vasculogenesis is disrupted, or do the CCM's play a role in Tie2 mediated regulation of vascular modeling? The latter is supported by recent zebrafish experiments. Zebrafish harboring mutations in the gene santa (san, homolog of krit1) resulted in increased Tie2 expression, suggesting san/krit1 is a negative regulator of endothelial cell gene expression. Zebrafish with the san mutation exhibit dilated vessels and an increase in endothelial cells similar to that observed in CCM1 knock-out embryos. Additionally, mutations of valentine (vtn, homolog of malcavernin) exhibit cardinal veins with decreased luminal diameter [52]. Further studies on the endothelial cell specific CCM3 knockout mouse are necessary to conclude the extent of phenocopy to CCM1 knockouts.

CCM3 in Glial affects cortical layering

In our mouse model, mice deficient of CCM3 in GFAP expressing cell lines exhibited severe difficulties with gait. Our nissl staining, in situ hybridization and immunohistochemistry revealed a lack of normal cortical and cerebellar layering. Although the cerebellar defects could account for the ataxia, this phenotype cannot be conclusively traced to the cerebellum given the extent of abnormal development throughout other brain regions, including the basal ganglia and somatosensory cortex. The question arises as to what is the cause of the observed dysmorphism? We have observed in previous experiments increased presence of GFAP signal in GFAP-Cre;CCM3$^{lox/lox}$ cortical sections. Does this represent an increased number of GFAP positive cells? Our BrdU experiments suggest the contrary. Fewer dividing cells were identified in the GFAP-Cre;CCM3$^{lox/lox}$ cortex. The observation of fewer dividing cells may be explained by the decrease in neuronal migration as revealed by in situ

hybridization. The cells which normally would be dividing in the cortex may never make it out of the ventricular zone. Or could the increase in GFAP signal represent increased astrocytic processes, since GFAP is an intermediate filament? It is possible that CCM3 modulates the extent and direction of glia process growth. A perturbation in this growth may lead to aberrant glial processes. If this is correct, and what we have observed are aberrant processes, this is suggestive of a problem in the normal communication glia usually undergo with the surrounding environment of extracellular matrix, neurons and endothelia. Moving forward, we will use TUNEL assays on cortical sections to observe changes in apoptosis.

GFAP-Cre;CCM3$^{lox/+}$ mice were the only available control mice for the BrdU experiments. In future experiments, comparisons made between WT and GFAP-Cre;CCM3$^{lox/lox}$ mice may reveal a greater difference in BrdU labeling in somatosensory cortex and possibly the visual cortex.

GFAP-Cre;CCM3$^{lox/lox}$ astrocyte cultures are resistant to apoptosis

We utilized flow activated cell sorting to observe apoptosis. This was the first time our group has attempted this technique. This method has significant advantages to other methods of observing apoptosis. With FACS we are able to observe the whole culture. This decreases the incidence of a sampling error, which may occur when choosing fields of a slide on which to perform counts. In the future, the use of FACS will allow us to sort cells based on expression of cell markers. After sorting, these cells will be used for RT-PCR and Western blotting to assess changes in expression of CCM pathway modulators.

In agreement with our previous PDCD10 siRNA experiments in HUVECs and TUNEL assays performed on primary GFAP-Cre;CCM3$^{lox/lox}$ astrocytes exposed to cycloheximide, GFAP-Cre;CCM3$^{lox/lox}$ astrocytes exhibit less expression of intracellular phospholipids on their outer surface than control astrocytes three hours after exposure to cycloheximide. We measured this expression of normally intracellular phospholipids by annexin V staining, a known marker of early apoptosis. Although our data reveals a trend towards resistance to apoptosis in the GFAP-Cre;CCM3$^{lox/lox}$ astrocytes, significance was not achieved. This experiment was complicated by a number of factors.

Analysis of the FACS dot plots reveals that the vast majority of culture, control and experimental, did not enter apoptosis after exposure to cycloheximide. There are at least two explanations for this observation. We introduced cycloheximide to cultures after the cultures had reached confluence. In other experiments using HUVECS, I have noticed a decrease in how responsive cultures are to an intervention (antibody or chemical) once allowed to grow to confluence. Cultures have been more responsive to intervention when the intervention is performed on cultures around 70-80% confluence. Future cycloheximide experiments should be performed before cultures reach confluence. Another explanation is that too little cycloheximide was used to induce apoptosis. We used 20 μg/ml of cycloheximide in culture to induce apoptosis. This concentration has been shown to induce apoptosis in approximately 50% of wild-type primary rat astrocyte cultures [53]. This is not terribly different from our ability to induce apoptosis in approximately 38% of GFAP-Cre;CCM3$^{lox/+}$ cultures. Increasing the concentration of cycloheximide used under our conditions may induce apoptosis in a higher percentage of the culture population. Unfortunately, heterozygous, GFAP-Cre;CCM3$^{lox/+}$, cultures

were the only available controls for this set of experiments. It would be interesting to investigate the difference between GFAP-Cre;CCM3$^{lox/lox}$ and WT cultures in response to apoptotic stimuli.

Another complicating factor in our experiments was the lack of purity in our astrocyte cultures. In many of our astrocyte cultures, immunohistochemistry for GFAP and staining of DAPI revealed a significant population of cells which were not GFAP positive. Our cultures were often contaminated with another cell type. The most common contaminant in primary astrocyte cultures are fibroblasts. In our system, fibroblasts from GFAP-Cre;CCM3$^{lox/lox}$ brains would normally express CCM3. These cells may not be resistant to apoptosis, as CCM3 deficient cells seem to be. The contamination of our cultures with fibroblast may have been responsible for the lack of consistent results as evident by the error bars in figure 8.

β-1 integrin modulation changed expression of a modulator of caspase-3

The literature has implicated CCM1 in β-1 integrin signaling through interactions with ICAP. Mounting evidence from our group and others suggest the CCM's act by modulating a common pathway and possibly as a complex. This present study further supports this hypothesis based on the similarities of phenotype between CCM1 mutant and our Tie2-CCM3 knock-outs. Additionally, our GFAP-Cre;CCM3$^{lox/lox}$ mice have demonstrated cortical layering perturbations similar to that seen in β1-integrin mutants [30].

To further pinpoint CCM3's role in β1-integrin signaling it will be necessary to be able to change β1-integrin signaling. This could be attempted by changing the substrate on which astrocyte cultures will be grown or changing β1-integrin expression.

The method we have chosen uses antibodies in cell culture to modify signaling of endogenously expressed β1-integrin. The ability to use P4C10, a known blocker of β1-integrin signaling, to attenuate caspase-3; coupled with the ability to utilize TS2/16, a known potentiator of β1-integrin signaling, to increase caspase-3 expression will allow us to further elucidate CCM3's role in β1-integrin mediated apoptosis, cell migration, adhesion and proliferation.

Conclusion

The above experiments further support the hypothesis that CCM3 is involved in a signaling pathway common to CCM1 and CCM2. Our Cre;lox mouse model has replicated human disease, producing CCM in the GFAP-Cre;CCM3$^{lox/lox}$ mouse, along with the dilated vessels often accompanying human CCM. The findings in the GFAP-Cre;CCM3$^{lox/lox}$ mouse suggest that CCM3 is important in glia for the prevention of CCM, as well as normal cortical development. Our mouse model differs from human CCM in the fact that all GFAP positive cells present in the mouse CNS are deficient in CCM3. In a two-hit hypothesis of familial human CCM, these cells would be haploinsufficient. The acquisition of an additional, random mutation of the functional allele could cause the development of CCM without gross abnormalities in cortical development.

Future experiments could utilize a Cre-recombinase expressing adenovirus. This virus injected into the CNS of Cre;CCM3$^{lox/lox}$ mice would afford us greater temporal and spatial control of CCM3 attenuation. It would be interesting to see if this method would

lead to CCM formation. It would also be interesting to know if loosing CCM3 function and subsequent CCM formation is dependent on the stage of development.

Our mouse model, combined with primary cell cultures obtained from our mice, has been useful in elucidating CCM3 function. With the discovery of a CCM in one of the mutant mice, this system may be a useful model of human disease. Our methods will continue to be useful in further clarifying the pathogenesis of cerebral cavernous malformations.

References

1. Dobyns, W.B., et al. 1987. Familial cavernous malformations of the central nervous system and retina. Ann Neurol. **21**(6): p. 578-83.
2. Eerola, I., et al. 2000. KRIT1 is mutated in hyperkeratotic cutaneous capillary-venous malformation associated with cerebral capillary malformation. Hum Mol Genet. **9**(9): p. 1351-5.
3. Mindea, S.A., et al. 2006. Cerebral cavernous malformations: clinical insights from genetic studies. Neurosurg Focus. **21**(1): p. e1.
4. Moriarity, J.L., R.E. Clatterbuck, and D. Rigamonti. 1999. The natural history of cavernous malformations. Neurosurg Clin N Am. **10**(3): p. 411-7.
5. Del Curling, O., Jr., D.L. Kelly, Jr., A.D. Elster, and T.E. Craven. 1991. An analysis of the natural history of cavernous angiomas. J Neurosurg. **75**(5): p. 702-8.
6. Zabramski, J.M., J.S. Henn, and S. Coons. 1999. Pathology of cerebral vascular malformations. Neurosurg Clin N Am. **10**(3): p. 395-410.
7. Robinson, J.R., I.A. Awad, and J.R. Little. 1991. Natural history of the cavernous angioma. J Neurosurg. **75**(5): p. 709-14.
8. Zabramski, J.M., et al. 1994. The natural history of familial cavernous malformations: results of an ongoing study. J Neurosurg. **80**(3): p. 422-32.
9. Laurans, M.S., et al. 2003. Mutational analysis of 206 families with cavernous malformations. J Neurosurg. **99**(1): p. 38-43.
10. Laberge-le Couteulx, S., et al. 1999. Truncating mutations in CCM1, encoding KRIT1, cause hereditary cavernous angiomas. Nat Genet. **23**(2): p. 189-93.
11. Gault, J., R. Shenkar, P. Recksiek, and I.A. Awad. 2005. Biallelic somatic and germ line CCM1 truncating mutations in a cerebral cavernous malformation lesion. Stroke. **36**(4): p. 872-4.
12. Serebriiskii, I., et al. 1997. Association of Krev-1/rap1a with Krit1, a novel ankyrin repeat-containing protein encoded by a gene mapping to 7q21-22. Oncogene. **15**(9): p. 1043-9.

13. Bos, J.L. 2005. Linking Rap to cell adhesion. Curr Opin Cell Biol. **17**(2): p. 123-8.
14. Caron, E. 2003. Cellular functions of the Rap1 GTP-binding protein: a pattern emerges. J Cell Sci. **116**(Pt 3): p. 435-40.
15. Kooistra, M.R., N. Dube, and J.L. Bos. 2007. Rap1: a key regulator in cell-cell junction formation. J Cell Sci. **120**(Pt 1): p. 17-22.
16. Katagiri, K., A. Maeda, M. Shimonaka, and T. Kinashi. 2003. RAPL, a Rap1-binding molecule that mediates Rap1-induced adhesion through spatial regulation of LFA-1. Nat Immunol. **4**(8): p. 741-8.
17. Beraud-Dufour, S., et al. 2007. Krit 1 interactions with microtubules and membranes are regulated by Rap1 and integrin cytoplasmic domain associated protein-1. Febs J. **274**(21): p. 5518-32.
18. Bretscher, A., K. Edwards, and R.G. Fehon. 2002. ERM proteins and merlin: integrators at the cell cortex. Nat Rev Mol Cell Biol. **3**(8): p. 586-99.
19. Craig, H.D., et al. 1998. Multilocus linkage identifies two new loci for a mendelian form of stroke, cerebral cavernous malformation, at 7p15-13 and 3q25.2-27. Hum Mol Genet. **7**(12): p. 1851-8.
20. Liquori, C.L., et al. 2003. Mutations in a gene encoding a novel protein containing a phosphotyrosine-binding domain cause type 2 cerebral cavernous malformations. Am J Hum Genet. **73**(6): p. 1459-64.
21. Sheikh-Hamad, D., et al. 1998. p38 kinase activity is essential for osmotic induction of mRNAs for HSP70 and transporter for organic solute betaine in Madin-Darby canine kidney cells. J Biol Chem. **273**(3): p. 1832-7.
22. Garmyn, M., et al. 2001. Human keratinocytes respond to osmotic stress by p38 map kinase regulated induction of HSP70 and HSP27. J Invest Dermatol. **117**(5): p. 1290-5.
23. Uhlik, M.T., et al. 2003. Rac-MEKK3-MKK3 scaffolding for p38 MAPK activation during hyperosmotic shock. Nat Cell Biol. **5**(12): p. 1104-10.
24. Zawistowski, J.S., et al. 2005. CCM1 and CCM2 protein interactions in cell signaling: implications for cerebral cavernous malformations pathogenesis. Hum Mol Genet. **14**(17): p. 2521-31.

25. Zhang, J., et al. 2001. Interaction between krit1 and icap1alpha infers perturbation of integrin beta1-mediated angiogenesis in the pathogenesis of cerebral cavernous malformation. Hum Mol Genet. **10**(25): p. 2953-60.
26. Seker, A., et al. 2006. CCM2 expression parallels that of CCM1. Stroke. **37**(2): p. 518-23.
27. Fournier, H.N., et al. 2005. Nuclear translocation of integrin cytoplasmic domain-associated protein 1 stimulates cellular proliferation. Mol Biol Cell. **16**(4): p. 1859-71.
28. Zhang, X.A. and M.E. Hemler. 1999. Interaction of the integrin beta1 cytoplasmic domain with ICAP-1 protein. J Biol Chem. **274**(1): p. 11-9.
29. Graus-Porta, D., et al. 2001. Beta1-class integrins regulate the development of laminae and folia in the cerebral and cerebellar cortex. Neuron. **31**(3): p. 367-79.
30. Belvindrah, R., et al. 2007. Beta1 integrins in radial glia but not in migrating neurons are essential for the formation of cell layers in the cerebral cortex. J Neurosci. **27**(50): p. 13854-65.
31. Bergametti, F., et al. 2005. Mutations within the programmed cell death 10 gene cause cerebral cavernous malformations. Am J Hum Genet. **76**(1): p. 42-51.
32. Guclu, B., et al. 2005. Mutations in apoptosis-related gene, PDCD10, cause cerebral cavernous malformation 3. Neurosurgery. **57**(5): p. 1008-13.
33. Wang, Y.G., H.T. Liu, Y.M. Zhang, and D.L. Ma. 1999. cDNA cloning and expression of an apoptosis-related gene, human TFAR-15 gene. Science in China series C-life sciences. **42**: p. 323-329.
34. Wu, Z., H. Jin, and Y. Gu. 2002. Changes of gene expression in atrophic muscle induced by brachial plexus injury in rats. Chin. J. Traumatol. **18**: p. 357-360.
35. Lu, X., et al. 2004. Tumor necrosis factor-related apoptosis-inducing ligand can induce apoptosis in subsets of premalignant cells. Am J Pathol. **165**(5): p. 1613-20.
36. Ma, X., et al. 2007. PDCD10 interacts with Ste20-related kinase MST4 to promote cell growth and transformation via modulation of the ERK pathway. Mol Biol Cell. **18**(6): p. 1965-78.

37. Lin, C.G., et al. 2005. Integrin-dependent functions of the angiogenic inducer NOV (CCN3): implication in wound healing. J Biol Chem. **280**(9): p. 8229-37.
38. Yee, K.L., V.M. Weaver, and D.A. Hammer. 2008. Integrin-mediated signalling through the MAP-kinase pathway. IET Syst Biol. **2**(1): p. 8-15.
39. Voss, K., et al. 2007. CCM3 interacts with CCM2 indicating common pathogenesis for cerebral cavernous malformations. Neurogenetics. **8**(4): p. 249-56.
40. Stahl, S., et al. 2008. Novel CCM1, CCM2, and CCM3 mutations in patients with cerebral cavernous malformations: in-frame deletion in CCM2 prevents formation of a CCM1/CCM2/CCM3 protein complex. Hum Mutat. **29**(5): p. 709-17.
41. Kisanuki, Y.Y., et al. 2001. Tie2-Cre transgenic mice: a new model for endothelial cell-lineage analysis in vivo. Dev Biol. **230**(2): p. 230-42.
42. Reddig, P.J. and R.L. Juliano. 2005. Clinging to life: cell to matrix adhesion and cell survival. Cancer Metastasis Rev. **24**(3): p. 425-39.
43. Oguey, D., P.W. George, and C. Ruegg. 2000. Disruption of integrin-dependent adhesion and survival of endothelial cells by recombinant adenovirus expressing isolated beta integrin cytoplasmic domains. Gene Ther. **7**(15): p. 1292-303.
44. Kagami, S. and S. Kondo. 2004. Beta1-integrins and glomerular injury. J Med Invest. **51**(1-2): p. 1-13.
45. Alvarez, B., P.J. Stroeken, M.J. Edel, and E. Roos. 2008. Integrin Cytoplasmic domain-Associated Protein-1 (ICAP-1) promotes migration of myoblasts and affects focal adhesions. J Cell Physiol. **214**(2): p. 474-82.
46. Ahlemeyer, B. and E. Baumgart-Vogt. 2005. Optimized protocols for the simultaneous preparation of primary neuronal cultures of the neocortex, hippocampus and cerebellum from individual newborn (P0.5) C57Bl/6J mice. J Neurosci Methods. **149**(2): p. 110-20.
47. Fukai, F., et al. 1998. Modulation of apoptotic cell death by extracellular matrix proteins and a fibronectin-derived antiadhesive peptide. Exp Cell Res. **242**(1): p. 92-9.

48. Calzada, M.J., et al. 2003. Recognition of the N-terminal modules of thrombospondin-1 and thrombospondin-2 by alpha6beta1 integrin. J Biol Chem. **278**(42): p. 40679-87.
49. Whitehead, K.J., et al. 2004. Ccm1 is required for arterial morphogenesis: implications for the etiology of human cavernous malformations. Development. **131**(6): p. 1437-48.
50. Urness, L.D., L.K. Sorensen, and D.Y. Li. 2000. Arteriovenous malformations in mice lacking activin receptor-like kinase-1. Nat Genet. **26**(3): p. 328-31.
51. Dominguez, M.G., et al. 2007. Vascular endothelial tyrosine phosphatase (VE-PTP)-null mice undergo vasculogenesis but die embryonically because of defects in angiogenesis. Proc Natl Acad Sci U S A. **104**(9): p. 3243-8.
52. Jin, S.W., et al. 2007. A transgene-assisted genetic screen identifies essential regulators of vascular development in vertebrate embryos. Dev Biol. **307**(1): p. 29-42.
53. Tsuchida, T., T. Kato, A. Yamada, and K. Kawamoto. 2002. Cycloheximide induces apoptosis of astrocytes. Pathol Int. **52**(3): p. 181-5.